

On the normal modes of freely vibrating elastic objects of various shapes

Jeffrey de Rue

March 1996



Parallel Scientific Computing and Simulation Group
Department of Mathematics, Computer Science, Physics and Astronomy
University of Amsterdam



Acknowledgments

This master of science thesis could not have been completed without the support of several people.

First of all I would like to thank Jan de Ronde because he invested the most time and effort in me. He guided me during my research and advised me in making this paper. Dick van Albada was also a great support because of his valuable comments on my research and on preliminary versions of this thesis. I would like to thank Peter Slood for giving me this interesting research topic and for supervising the project. My gratitude goes to all the members of the PSC&S group for giving me a pleasant time and supporting me. In this context I have to mention Martin Bergman who was always obliged to give me technical support.

This leaves me with the two most important persons during my time at university. I'm referring to my parents who made sure that I had nothing to worry about but my study. They have always given me full support.

To Hans



Contents

I	Introductory Chapters	7
1	Introduction	9
1.1	Context of the project	9
1.2	Aim of the project	10
1.3	Structure of the paper	11
2	Theory of elasticity	13
2.1	Infinitesimal affine transformations	13
2.2	Equations of equilibrium of forces	15
2.3	Stress - strain relations	17
2.4	Equations of motion	18
II	Analytical Solutions for Elastic Spheres	21
3	Solutions of the equation of motion for a homogeneous isotropic sphere	23
3.1	Spherical solid harmonics	23
3.2	Solutions for a vibrating sphere by means of spherical harmonics	24
3.3	Boundary conditions and frequency equations for a vibrating sphere	27
3.4	Vibrations of the first class	28
3.5	Vibrations of the second class	29
4	Quadrupole modes	33
4.1	Frequencies of the quadrupole modes	33
4.2	Expressions for the displacements	33
4.3	Visualization of the modes	36
4.4	Deviations of the frequency	38
III	Variational Methods	43
5	A variational approach to approximate the normal modes of elastic objects	45
5.1	Hamilton's principle applied to elasticity theory	45
5.2	Numerical algorithm	46

6 Applications of the approximation method	49
6.1 A solid sphere	49
6.2 Prolate and oblate spheroids	50
6.3 A concentric hole	52
6.4 A bore hole	55
6.5 Comparison with experimental data	57
IV Conclusions	59
7 Concluding remarks and summary	61
V Appendices	63
A Additional plots	65
B Documentation for the computer programs	69
B.1 Numerical approximation	69
B.2 Analytical solutions	70
Bibliography	73

Part I

Introductory Chapters

Chapter 1

Introduction

1.1 Context of the project

The existence of gravitational radiation is predicted by Albert Einstein in his theory of General Relativity. If we could detect this radiation the use would be twofold. In the first place it provides us with one of the most fundamental tests of Einstein's theory. In the second place it opens a whole new window on the universe. We are already familiar with the detection of electromagnetic radiation. We hope to get more information on the universal structure with the aid of the detection of these gravity waves. This is likely because gravitational waves are almost unaffected by matter and therefore they can travel long distances without being disturbed. However, this lack of interaction with matter also makes the waves hard to detect. The expectation is that only the waves caused by binary stars (i.e. two stars rotating about each other), supernovas and black holes will be strong enough to detect.

In 1993 prof. G. Frossati from the university of Leiden raised the idea to build a *spherical resonant-mass antenna*. This antenna should be able to detect gravitational radiation arriving at earth from extra galactic sources. This project is known as GRAIL* .

The antenna will consist of a sphere suspended in vacuum. This sphere is expected to vibrate with a very small amplitude ($\sim 10^{-21}$ m) because of the impinging gravitational waves. A drawing of this GRAIL antenna is displayed in figure 1.1. The sphere will be made of a copper alloy of which the exact composition is still under investigation and have a diameter of three metres. The total mass will be about 10^5 kg. Because of the tiny amplitudes special care must be taken to reduce noise. To reduce the thermal noise it has to be cooled to a temperature below 100 mK. The suspension has to attain an attenuation of at least 320 dB (a factor 10^{16}) because of noise from the outside world. Transducers will be attached to the surface of the sphere to detect the vibrations. An analysis of the electric signals from these transducers must give us information about the radiation which impinged on the sphere. The detector should be operational in the year 2001 and the total costs are estimated at about 45 million Dutch guilder (about 28 million US \$).

*GRAIL stands for Gravitational Radiation Antenna in Leiden. The participating academic institutes are RUL, UT, TUE, UvA, NIKHEF/FOM, SRON and ESA/ESTEC.

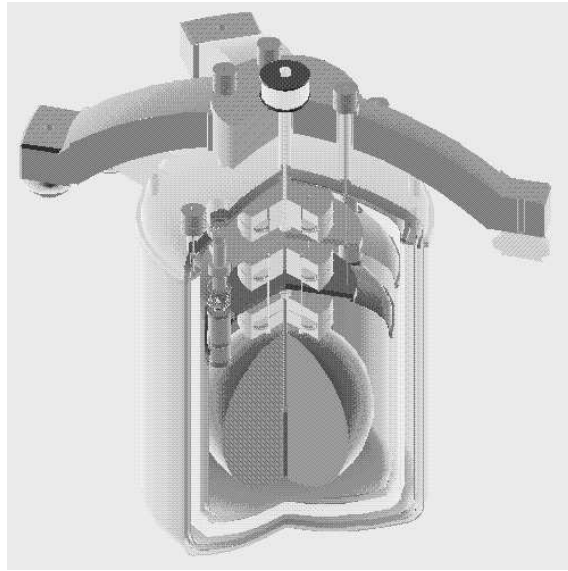


Figure 1.1: A drawing of the GRAIL sphere in a heat-isolating vacuum chamber. On top the concrete arms to which it is suspended are visible.

1.2 Aim of the project

Gravitational waves will excite the *quadrupole* normal modes of the sphere (see [8] and [16]). The frequencies and shapes of these modes were deduced analytically for a freely vibrating perfect sphere over 50 years ago [9]. In our case we don't have a freely vibrating perfect sphere for a number of reasons:

- The sphere has to be suspended, so it is not freely vibrating.
- There is a hole through the sphere. In this hole a rod is placed to make the sphere rest approximately at its centre of mass.
- It is impossible to cast such a large sphere perfectly. Therefore there will be small deviations of the spherical shape.
- The sphere will be deformed by its own weight, so it will become kind of a 'pear'.
- Transducers will be attached to the sphere to measure the vibrations.

It is the task of our group to investigate the effects of the above points on the normal modes.

In this thesis we will show the analytical solutions for the elastic vibrations of a homogeneous isotropic sphere first. As we will see, the derivation of the solutions is rather tedious. It is presumably impossible to give an analytical solution for a system with all the deviations from a spherical shape that we have at hand here. Therefore the procedure of a numerical calculation to approximate the normal modes of various elastic objects will be described. This procedure can be applied to various shapes, among others a sphere, an ellipsoid and a sphere with a hole through it. The computationally very intensive calculations will be carried out on a CRAY C98 supercomputer.

The results from these calculations can be used in two ways. In the first place it may be possible to examine some of the influences on the normal modes mentioned above. In the second place the results will be used to validate a finite element simulation which is also performed in our group. With the finite element simulation it will be possible to investigate more of the factors mentioned above.

1.3 Structure of the paper

The vibrations under consideration are forced elastic vibrations. Therefore we will discuss the theory of elasticity first. Several general equations are deduced which rule the vibrations. This is done in chapter 2.

In chapter 3 we are going to solve these equations analytically for the case of a homogeneous isotropic sphere.

In chapter 4 we confine our attention to a special case of the solutions. We consider the quadrupole modes of a sphere here because these modes are expected to interact with the gravitational radiation field (see e.g. [8] and [16]).

The numerical approximation procedure is introduced in chapter 5 and applied in chapter 6.

A few plots additional to chapter 3 are shown in appendix A. The expressions plotted here determine the allowed frequencies of the normal modes of a freely vibrating sphere.

Finally, a description how to use the computer programs to calculate the normal modes is given in appendix B.



Chapter 2

Theory of elasticity

The theory discussed in this chapter can be found in any textbook on elasticity theory, for example [14]. The basic rules that we encounter here will be used in the other chapters.

2.1 Infinitesimal affine transformations

We consider transformations of a vector \mathbf{A} by describing the change in the components A_i ($i = 1, 2, 3$) along the coordinate axes. A coordinate A_i is transformed into A'_i and the difference is called δA_i :

$$\delta A_i \equiv A'_i - A_i = \alpha_{ij} A_j \quad (2.1)$$

The coefficients α_{ij} may be dependent on the coordinates. Take note that a repeated index indicates summation as the index that is repeated takes the values 1,2,3, i.e. $\alpha_{1j} A_j = \alpha_{11} A_1 + \alpha_{12} A_2 + \alpha_{13} A_3$. This is called the summation convention. A transformation of this type is called an *infinitesimal affine transformation* if the coefficients α_{ij} are so small that their products can be neglected in comparison with their first powers. If two infinitesimal affine transformations like (2.1) are performed, the resulting transformation can be found by just adding the coefficients of the transformations. So if the first transformation has coefficients $\alpha_{ij}^{(1)}$ and causes a difference $\delta A_i^{(1)}$ and the second transformation has coefficients $\alpha_{ij}^{(2)}$ and causes a difference $\delta A_i^{(2)}$ the resulting transformation is given by:

$$\delta A_i = \delta A_i^{(1)} + \delta A_i^{(2)} = \alpha_{ij}^{(1)} A_j + \alpha_{ij}^{(2)} A_j = (\alpha_{ij}^{(1)} + \alpha_{ij}^{(2)}) A_j = \alpha_{ij} A_j \quad (2.2)$$

From this we see that the order in which the transformations are performed doesn't influence the result. So we can always decompose a transformation like (2.1) into other transformations. Doing this in a special way we obtain:

$$\delta A_i = \alpha_{ij} A_j = \left[\frac{1}{2}(\alpha_{ij} + \alpha_{ji}) + \frac{1}{2}(\alpha_{ij} - \alpha_{ji}) \right] A_j \quad (2.3)$$

We call the first coefficients e_{ij} :

$$e_{ij} = e_{ji} \equiv \frac{1}{2}(\alpha_{ij} + \alpha_{ji}) \quad (2.4)$$

So these coefficients are symmetric and therefore the transformation $\delta A_i = e_{ij} A_j$ corresponds to pure deformation of the body under consideration. The coefficients e_{ij} are called components of the *strain tensor*. A body is strained when the relative position of points in it is altered.

On the contrary the second coefficients are *skew-symmetric*:

$$\omega_{ij} = -\omega_{ji} \equiv \frac{1}{2}(\alpha_{ij} - \alpha_{ji}) \quad (2.5)$$

The transformation $\delta A_i = \omega_{ij} A_j$ represents rigid body motion. We will show that this follows from the skew-symmetry of the coefficients ω_{ij} now. Rigid body motion implies that the length of any vector in the body doesn't change: $|\mathbf{A} + \delta \mathbf{A}| = |\mathbf{A}|$. By using $\delta A_i = \frac{1}{2}(\alpha_{ij} - \alpha_{ji}) A_j$ it follows from this condition of conservation of length that

$$[A_i + \frac{1}{2}(\alpha_{ij} - \alpha_{ji}) A_j]^2 = A_i^2 \quad (2.6)$$

After working out the square root and neglecting all products of coefficients α_{ij} we obtain

$$\alpha_{ij} A_i A_j = \alpha_{ji} A_j A_i \quad (2.7)$$

This condition is always true since the indices are only dummies because the summation convention is used. So when we use the coefficients (2.5), the length of any vector in the body is conserved. This implies that the coefficients (2.5) correspond with rigid body motion.

Now we introduce the displacement of the point (x_1^0, x_2^0, x_3^0) in a continuous medium. If this point is at $(x_1^{0'}, x_2^{0'}, x_3^{0'})$ after a deformation, we can define the displacement by:

$$u_i(x_1^0, x_2^0, x_3^0) = x_i^{0'} - x_i^0 \quad (2.8)$$

Some other point (x_1, x_2, x_3) in the neighbourhood will transform into (x_1', x_2', x_3') . Hence a vector \mathbf{A} which initially runs from (x_1^0, x_2^0, x_3^0) to (x_1, x_2, x_3) will be deformed into a vector \mathbf{A}' which runs from $(x_1^{0'}, x_2^{0'}, x_3^{0'})$ to (x_1', x_2', x_3') . With this knowledge we are able to write down an expression for the components of $\delta \mathbf{A} = \mathbf{A}' - \mathbf{A}$:

$$\begin{aligned} \delta A_i &= (x_i' - x_i^{0'}) - (x_i - x_i^0) \\ &= (x_i' - x_i) - (x_i^{0'} - x_i^0) \\ &= u_i(x_1^0 + A_1, x_2^0 + A_2, x_3^0 + A_3) - u_i(x_1^0, x_2^0, x_3^0) \\ &= \left(\frac{\partial u_i}{\partial x_j} \right)_0 A_j \end{aligned}$$

We have neglected the higher order terms in the Taylor's expansion of the function $u_i(x_1^0 + A_1, x_2^0 + A_2, x_3^0 + A_3)$ in the last line. Introducing the short notation

$$\frac{\partial u_i}{\partial x_j} \equiv u_{i,j}$$

we can write:

$$\delta A_i = u_{i,j} A_j \quad (2.9)$$

Comparing (2.9) with (2.1) we see that $u_{i,j}$ has the same use as α_{ij} . If we assume that the displacements u_i as well as their partial derivatives are small we can conclude that (2.9) again defines an infinitesimal affine transformation which we can decompose into pure deformation and rigid body motion:

$$\delta A_i = u_{i,j} A_j = \left[\frac{1}{2}(u_{i,j} + u_{j,i}) + \frac{1}{2}(u_{i,j} - u_{j,i}) \right] A_j = (e_{ij} + \omega_{ij}) A_j \quad (2.10)$$

where

$$e_{ij} = \frac{1}{2}(u_{i,j} + u_{j,i}) \quad (2.11)$$

and

$$\omega_{ij} = \frac{1}{2}(u_{i,j} - u_{j,i}) \quad (2.12)$$

2.2 Equations of equilibrium of forces

There are mainly two kinds of forces which can act on a continuous medium. At first there are the volume forces which are proportional to the mass contained in the volume element $\Delta\tau$. We will represent these forces by the vector \mathbf{F} . At second there are the surface forces. These forces act on the surface $\Delta\sigma$ of the volume element $\Delta\tau$. The surface forces per unit area are represented by the *stress vector* \mathbf{T} . The stress vector is closely related to the nine components of the *stress tensor* τ_{ij} . These are defined as follows. Let $\overset{i}{\mathbf{T}}$ denote the stress vector acting on a planar surface element normal to the x_i -axis. So the resolution of the vector $\overset{i}{\mathbf{T}}$ into components along the coordinate axes gives $\overset{i}{\mathbf{T}} = \mathbf{e}_j \overset{i}{T}_j$, with \mathbf{e}_j the unit vector in the direction of the x_j -axis. The convenience of the notation

$$\overset{i}{\mathbf{T}}_j \equiv \tau_{ij} \quad (2.13)$$

should be clear now, because we can write with this:

$$\overset{i}{\mathbf{T}} = \mathbf{e}_j \tau_{ij} \quad (2.14)$$

To interpret the quantity τ_{ij} we must notice that this tension acts on a surface perpendicular to the x_i -axis. The second index indicates the direction of the stress. So for $i = j$ we have a tension that acts normal to the surface and for $i \neq j$ the stress acts in the plane perpendicular to the x_i -axis.

It is also possible to write down the components of the stress vector in terms of the components of the unit normal $\boldsymbol{\nu}$ to the surface element $\Delta\sigma$:

$$T_i = \tau_{ij} \nu_j \quad (2.15)$$

To obtain the equations of equilibrium we state that the resultant force acting on a continuous medium should be zero for each component. To do this we must integrate the body forces over all occupied space and the surface forces over the surface of the body:

$$\int_{\tau} F_i d\tau + \int_{\sigma} T_i d\sigma = \int_{\tau} F_i d\tau + \int_{\sigma} \tau_{ij} \nu_j d\sigma = 0$$

where we have used (2.15). As before we define a short notation for the partial derivative:

$$\tau_{ji,k} \equiv \frac{\partial \tau_{ji}}{\partial x_k}$$

With the aid of the divergence theorem of Gauss* we can rewrite the surface integral into a volume integral:

$$\int_{\sigma} \tau_{ij} \nu_j d\sigma = \int_{\tau} \tau_{ij,j} d\tau$$

Hence we obtain

$$\int_{\tau} (F_i + \tau_{ij,j}) d\tau = 0$$

which has to hold for every region τ . Thus at every interior point the equilibrium equation

$$F_i + \tau_{ij,j} = 0 \quad (2.16)$$

must be satisfied.

In a comparable manner we can show that the stress tensor is symmetric: $\tau_{ij} = \tau_{ji}$. Now we don't set the total force but the total torque (or moment of the force) due to body forces and surface forces with respect to a randomly chosen point equal to zero (as in [7]):

$$\int_{\tau} \epsilon_{ijk} x_j F_k d\tau + \int_{\sigma} \epsilon_{ijk} x_j T_k d\sigma = 0 \quad (2.17)$$

ϵ_{ijk} is the Levi-Civita tensor density and equals +1 if i, j, k is equal to 1,2,3 or a cyclic permutation of this row (so 2,3,1 or 3,1,2). It equals -1 if the i, j, k are different and the order 1,2,3 is changed in an a-cyclic way. It equals zero if two of the indices are equal. So with the aid of ϵ_{ijk} we have written the cross product in tensor notation. When we substitute (2.15) and use the Gauss theorem again we obtain

$$\int_{\tau} \epsilon_{ijk} x_j F_k d\tau + \int_{\sigma} \epsilon_{ijk} x_j \tau_{kl} \nu_l d\sigma = \int_{\tau} \epsilon_{ijk} x_j F_k d\tau + \int_{\tau} (\epsilon_{ijk} x_j \tau_{kl})_{,l} d\tau = 0 \quad (2.18)$$

Working out the derivative and setting $x_{j,l} = \delta_{jl}$ we obtain

$$\int_{\tau} \epsilon_{ijk} x_j (F_k + \tau_{kl,l}) d\tau + \int_{\tau} \epsilon_{ijk} \delta_{jl} \tau_{kl} d\tau = 0 \quad (2.19)$$

The first integral equals zero because of (2.16). When we take into account that the volume can be chosen arbitrarily it follows that the integrand in the second integral must vanish. This implicates that

$$\tau_{kl} = \tau_{lk} \quad (2.20)$$

*In conventional notation the Gauss theorem states:

$$\int_{\tau} \nabla \cdot \mathbf{A} d\tau = \int_{\sigma} \mathbf{A} \cdot \boldsymbol{\nu} d\sigma$$

which takes the form:

$$\int_{\tau} A_{i,i} d\tau = \int_{\sigma} A_i \nu_i d\sigma$$

2.3 Stress - strain relations

The *dilatation* is defined as:

$$\vartheta \equiv e_{ii} = u_{i,i} \quad (2.21)$$

The last step can be verified by looking at (2.11). The dilatation represents the expansion of a unit volume due to strain produced in the medium.

We shall assume that – at a fixed temperature – there exists a one-to-one analytic relation between the components of the stress tensor and the strain tensor. This relation is called the *generalized Hooke's law*. When it is expanded and we keep only the linear terms there remains:

$$\tau_{ij} = c_{ijkl}e_{kl} \quad (2.22)$$

A medium is called *elastically homogeneous* if the coefficients c_{ijkl} are independent of the position in the medium. Without loss in generality we can state that the c_{ijkl} are symmetric with respect to the first two components as well as with respect to the second two components. This leaves us with at most 36 independent constants while we had 81 coefficients. So this is the time to introduce a new notation with fewer indices. Our new indices will run from 1 to 6 so it suffices to give each of the 36 constants two indices. Consequently, the number of indices of the stress and the strain will diminish from two to one. The new notation is defined as follows:

$$\begin{aligned} \tau_{11} = \tau_1 \quad \tau_{22} = \tau_2 \quad \tau_{33} = \tau_3 \quad \tau_{23} = \tau_4 \quad \tau_{31} = \tau_5 \quad \tau_{12} = \tau_6 \\ e_{11} = e_1 \quad e_{22} = e_2 \quad e_{33} = e_3 \quad 2e_{23} = e_4 \quad 2e_{31} = e_5 \quad 2e_{12} = e_6 \end{aligned}$$

With this (2.22) becomes:

$$\tau_i = c_{ij}e_j \quad (i, j = 1, 2, \dots, 6) \quad (2.23)$$

The constants c_{ij} are called the *elastic constants* or *moduli* of the material.

It can be deduced [9] from the first law of thermodynamics that the *strain-energy density function* exists for a process that takes place adiabatically. This function is given by

$$W = \frac{1}{2}c_{ij}e_i e_j \quad (2.24)$$

It has the property

$$\frac{\partial W}{\partial e_i} = \tau_i. \quad (2.25)$$

Evaluation of the derivative and substituting for τ_i the expression from (2.23) gives $c_{ij} = c_{ji}$ and this reduces the number of independent elastic constants to 21.

There are a few special cases to be considered. Symmetry with respect to a plane reduces the number of independent elastic constants to 13. When we have symmetry with respect to three mutually perpendicular planes this number reduces to 9. When the elastic properties of a body are identical in all directions we say that the body is *isotropic*. The number of essential elastic constants diminishes to 2 in that case. This can be shown by imposing invariance of the coefficients under rotations about the axes. The two independent constants we will use are denoted by λ and μ and are called the *Lamé constants*. They are

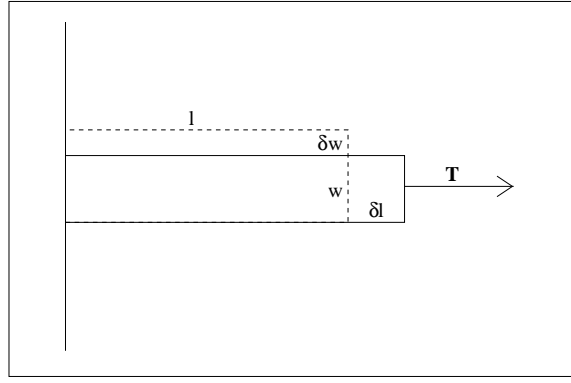


Figure 2.1: Illustration of the Poisson ratio σ and Young's modulus E . A bar with initial width w and length l is stretched by a stress \mathbf{T} . The length is increased with δl and the width is decreased with δw , $\sigma = \frac{\delta w}{w} \frac{l}{\delta l}$ and $E = \frac{\mathbf{T}l}{\delta l}$.

related to the elastic moduli by $c_{11} = \lambda + 2\mu$, $c_{12} = \lambda$ and $c_{44} = \mu$. The generalized Hooke's law for a homogeneous isotropic body can be written in the following form:

$$\tau_{ij} = \lambda \delta_{ij} \vartheta + 2\mu e_{ij} \quad (2.26)$$

The quantity μ is called the *modulus of rigidity* or the *shear modulus*. It suffices to have two independent elastic constants. Instead of the Lamé constants it is possible to use two other quantities which are called the *Young's modulus* E and the *Poisson ratio* σ . The transformation is given by

$$\lambda = \frac{E\sigma}{(1+\sigma)(1-2\sigma)} \quad \text{or} \quad \sigma \equiv \frac{\lambda}{2(\lambda + \mu)} \quad (2.27)$$

$$\mu = \frac{E}{2(1+\sigma)} \quad E \equiv \frac{\mu(3\lambda + 2\mu)}{\lambda + \mu} \quad (2.28)$$

The two quantities both have a physical interpretation. E represents the ratio of the tensile stress to the extension it produces. For a cylinder σ denotes the ratio of the contraction of an element perpendicular to the axis of the cylinder to the extension of the cylinder. This is illustrated in figure (2.1). The constants as well as the densities ρ of a few materials are listed in table 2.1 which is taken from [6].

2.4 Equations of motion

To obtain the equations of motion we set the resultant force which is calculated in (2.16) equal to the inertial force $\rho \ddot{u}_i$, with ρ the mass density and

$$\frac{\partial^2 u_i}{\partial t^2} \equiv \ddot{u}_i$$

This is called d'Alemberts principle. Hence we obtain

$$\tau_{ij,j} + F_i = \rho \ddot{u}_i \quad (2.29)$$

material	λ (GPa)	μ (GPa)	σ	E (GPa)	ρ (kg/m ³)
Aluminum	58.2	26.1	0.345	70.3	2706.5
Brass (70 Zn, 30 Cu)	86.9	37.3	0.350	100.6	7674
Cadmium	28.8	19.2	0.300	49.9	8647
Chromium	83.5	115.4	0.210	279.1	7194
Copper	105.6	48.3	0.343	129.8	8933
Gold	198.6	27.0	0.44	78.0	19281
Lead	41.0	5.59	0.44	16.1	11343

Table 2.1: The elastic constants and the densities for a few materials at 293 K.

Now we can eliminate τ_{ij} in favour of u_i . We start by substituting (2.11) in (2.26):

$$\tau_{ij} = \lambda \delta_{ij} u_{k,k} + \mu (u_{i,j} + u_{j,i}) \quad (2.30)$$

and this resulting expression for τ_{ij} is substituted in (2.29). We obtain for a homogeneous isotropic elastic solid:

$$\mu u_{i,jj} + (\lambda + \mu) u_{j,ji} + F_i = \rho \ddot{u}_i \quad (2.31)$$

or

$$\mu \nabla^2 u_i + (\lambda + \mu) \vartheta_{,i} + F_i = \rho \ddot{u}_i \quad (2.32)$$

This equation is also called the *Navier equation*.

Part II

Analytical Solutions for Elastic Spheres

Chapter 3

Solutions of the equation of motion for a homogeneous isotropic sphere

3.1 Spherical solid harmonics

In equilibrium in the absence of body forces we have from (2.32):

$$(\lambda + \mu)\vartheta_{,i} + \mu\nabla^2 u_i = 0 \quad (3.1)$$

Differentiating with respect to x_i we obtain $(\lambda + 2\mu)\nabla^2 \vartheta = 0$, so we must conclude:

$$\nabla^2 \vartheta = 0 \quad (3.2)$$

Because ϑ satisfies the Laplace equation we say that it is a *harmonic* function.

We are interested in solutions of the equations of motion which are (a combination of) *spherical solid harmonics*. These are functions which satisfy the Laplace equation and are rational homogeneous functions of the x_i of positive or negative integral degree n . The latter condition imposes that the functions, which we shall denote by V_n , are of the form

$$V_n = a_{klm} x_1^k x_2^l x_3^m$$

No summation convention should be used in this expression. The numbers a, k, l and m are of constant integer value and $k + l + m = n$.

We will make use of spherical coordinates. The transformation is defined as

$$\begin{aligned} x_1 &= r \sin \theta \cos \phi \\ x_2 &= r \sin \theta \sin \phi \\ x_3 &= r \cos \theta \end{aligned}$$

$$r \geq 0; \quad 0 \leq \theta \leq \pi; \quad 0 \leq \phi < 2\pi$$

where r represents the distance to the origin of the coordinate system. In these new coordinates V_n is of the form $r^n S_n$ with $S_n = S_n(\theta, \phi)$. $S_n(\theta, \phi)$ is called the *surface harmonic* or the *zonal harmonic*. The S_n are equal to the $P_n^0(\cos \theta)$ which are Legendre polynomials. The

general form for a spherical solid harmonic can be obtained by solving the Laplace equation with the method of separating variables. (See for example [12].) In this way the solutions become

$$Cr^n e^{im\phi} P_n^m(\cos\theta) = r^n Y_n^m(\theta, \phi) \quad (3.3)$$

where C is a normalization constant. There is a restriction for the integer value of m : $-n \leq m \leq n$. The $Y_n^m(\theta, \phi)$ are spherical harmonics for which an explicit expression can be looked up in a table.

It is possible to derive some formulas for the spherical solid harmonic functions V_n . These relations are listed below.

$$\nabla^2(x_i V_n) = 2V_{n,i} \quad (3.4)$$

$$\nabla^2(r^m V_n) = m(m+2n+1)r^{m-2}V_n \quad (3.5)$$

$$\nabla^2(r^m V_{n,i}) = m(m+2n-1)r^{m-2}V_{n,i} \quad (3.6)$$

$$x_i V_{n,i} = nV_n \quad (3.7)$$

$$x_i V_n = \frac{r^2}{2n+1} \left[V_{n,i} - r^{2n+1} \left(\frac{V_n}{r^{2n+1}} \right)_{,i} \right] \quad (3.8)$$

It is always possible to add solutions of the differential equation. The solutions are built up by spherical solid harmonics. There are three types of spherical solid harmonics which we will frequently encounter:

- Type ω . This type of spherical solid harmonic occurs in the solution in the following manner:

$$u_i = r^2 \omega_{n,i} + \alpha_n x_i \omega_n \quad (3.9)$$

α_n depends on n , λ and μ and can be evaluated by substituting (3.9) into (3.1).

- Type ϕ . This type contributes the following terms to the displacement:

$$u_i = \phi_{n,i} \quad (3.10)$$

- Type χ . This type contributes the following terms to the displacement:

$$u_i = \epsilon_{ijk} x_j \chi_{n,k} \quad (3.11)$$

The three displacements (3.9), (3.10) and (3.11) all satisfy (3.1).

3.2 Solutions for a vibrating sphere by means of spherical harmonics

In this section we will describe a derivation of the solution of the equation of motion as it can be found in [9]. We assume that the motion of every particle of the sphere is simple harmonic with a constant frequency. We denote the angular frequency by p . In this way we can take

$$u_i = u'_i \cos(pt + \epsilon) \quad (3.12)$$

Here the u'_i are functions of the x_i but not of the time t . The constant ϵ is independent of the x_i and only influences the phase of the vibration. The same shape is reached at different times with varying ϵ . Now we substitute this expression in (2.32) and take $F_i = 0$. Hence we obtain:

$$\mu \nabla^2 u_i + (\lambda + \mu) \vartheta_{,i} + \rho p^2 u_i = 0 \quad (3.13)$$

Here we have omitted the accent of u'_i . Since equation (3.13) holds for both u_i and u'_i , we may restore at any time the factor $\cos(pt + \epsilon)$ in the solution. Differentiating (3.13) with respect to x_i we obtain

$$(\nabla^2 + h^2) \vartheta = 0 \quad (3.14)$$

where $h^2 = \frac{p^2 \rho}{\lambda + 2\mu}$. Equation (3.13) can be rewritten as

$$(\nabla^2 + \kappa^2) u_i = \left(1 - \frac{\kappa^2}{h^2}\right) \vartheta_{,i} \quad (3.15)$$

where $\kappa^2 = \frac{p^2 \rho}{\mu}$. One solution of (3.15) is

$$u_i^{(1)} = -\frac{1}{h^2} \vartheta_{,i} \quad (3.16)$$

This can be verified by substituting this solution into (3.15). What remains is $(\nabla^2 + h^2) \vartheta_{,i} = 0$, and this relation holds because of (3.14). A more complete solution is obtained by adding to solution (3.16) solutions of the system of equations.

$$(\nabla^2 + \kappa^2) u_i = 0 \quad (3.17)$$

and

$$\vartheta = u_{i,i} = 0 \quad (3.18)$$

If we call the solutions of this system of equations $u_i^{(2)}$ we can write the total solution of (3.13) as

$$u_i = (u_i^{(1)} + u_i^{(2)}) \cos(pt + \epsilon) \quad (3.19)$$

To obtain this total solution we have to find a ϑ which satisfies (3.14) first. Then we can calculate $u_i^{(1)}$ by means of (3.16). Finally we must solve the system (3.17) and (3.18) and add the solution to $u_i^{(1)}$.

To solve (3.14) we suppose $\vartheta = R_n(r) S_n(\theta, \phi)$, so separation of variables again. S_n is a spherical surface harmonic of degree n . After writing (3.14) in spherical coordinates and separating variables we obtain

$$\left(\frac{\partial^2}{\partial r^2} + h^2 - \frac{n(n+1)}{r^2} \right) (r R_n) = 0 \quad (3.20)$$

which can be shown to have the following solution:

$$r R_n = r^{n+1} \left(\frac{1}{r} \frac{\partial}{\partial r} \right)^n \frac{A_n \sin(hr) + B_n \cos(hr)}{r} \quad (3.21)$$

where A_n and B_n are arbitrary constants. Now we take for ϑ :

$$\vartheta = \sum_n \omega_n \psi_n(hr) \quad (3.22)$$

where ω_n is a spherical solid harmonic. $\psi_n(x)$ is given by:

$$\psi_n(x) = \left(\frac{1}{x} \frac{\partial}{\partial x} \right)^n \frac{\sin x}{x} \quad (3.23)$$

Note that we have dropped the part $\cos(hr)/r$ from the solution to get a physically valid solution for $r \rightarrow 0$. The functions $\psi_n(x)$ are closely related to the spherical Bessel functions of the first kind $j_n(x)$:

$$j_n(x) = (-x)^n \psi_n(x) \quad (3.24)$$

Two important relations for ψ_n are the differential equation

$$\left(\frac{d^2}{dx^2} + \frac{2(n+1)}{x} \frac{d}{dx} + 1 \right) \psi_n(x) = 0 \quad (3.25)$$

and the relation for consecutive values of n

$$x \frac{d\psi_{n-1}(x)}{dx} = x^2 \psi_n(x) = -\psi_{n-2}(x) - (2n-1)\psi_{n-1}(x). \quad (3.26)$$

We can write down an expression for $u_i^{(2)}$ in the same manner as for ϑ because (3.17) has the same form as (3.14):

$$u_i^{(2)} = U_{ni} \psi_n(\kappa r) \quad (3.27)$$

The U_{ni} are again spherical solid harmonics of degree n. But now (3.18) has to be satisfied also. One way of doing so is taking

$$U_{ni} = \epsilon_{ijk} x_j \chi_{n,k} \quad (3.28)$$

A second way is taking the curl of (3.27) with U_{ni} given by (3.28). This solution is allowed because the curl of u_i also satisfies the system (3.17) and (3.18). In this way we obtain after rewriting with the aid of (3.8) and (3.26):

$$\epsilon_{ijk} u_j^{(2)} u_k^{(2)} = \frac{n+1}{2n+1} \psi(\kappa r) \chi_{n,i} - \frac{n}{2n+1} \psi_{n+1}(\kappa r) \kappa^2 r^{2n+3} \left(\frac{\chi_n}{r^{2n+1}} \right)_{,i} \quad (3.29)$$

The spherical solid harmonic that occurs in this solution is of the ϕ type, so we replace χ_n by ϕ_n . We can add the solutions (3.16) with ϑ given by (3.22), (3.27) with U_{ni} given by (3.28) and (3.29) now to write for the solution of (3.15)

$$u_i = \sum_n \left[-\frac{1}{h^2} [\omega_n \psi_n(hr)]_{,i} + \psi_n(\kappa r) (\epsilon_{ijk} x_j \chi_{n,k} + \phi_{n+1,i}) - \frac{n+1}{n+2} \psi_{n+2}(\kappa r) \kappa^2 r^{2n+5} \left(\frac{\phi_{n+1}}{r^{2n+3}} \right)_{,i} \right] \quad (3.30)$$

3.3 Boundary conditions and frequency equations for a vibrating sphere

First we derive a formula for the boundary conditions because they determine the frequency equations. Only certain values for the frequency are allowed by these latter equations.

The boundary conditions we impose are *traction boundary conditions*. This means that the sphere is maintained in equilibrium by applying suitable surface tractions on its boundary. The conditions involve the stress tensor. Since no forces act on the surface of the sphere we say that the boundaries are traction free and the applied surface traction vanishes. We have for the components along the x_i axis of the traction across a surface $r=\text{constant}$

$$\begin{aligned} \frac{1}{r}x_j\tau_{ij} &= \frac{1}{r}[\lambda x_i u_{k,k} + \mu[(x_j u_j)_{,i} - u_i + x_j u_{i,j}]] \\ &= \frac{1}{r}\left[\lambda x_i \vartheta + \mu(x_j u_j)_{,i} + \mu\left(r\frac{\partial u_i}{\partial r} - u_i\right)\right] \end{aligned} \quad (3.31)$$

Where we have used (2.30) in the second step. The boundary conditions imply that these tractions vanish at the surface of the sphere. So we have to impose that (3.31) equals zero for $r = a$, where a denotes the radius of the sphere. When we substitute for ϑ the expression from (3.22) and for u_i the form obtained in (3.30) we obtain after tedious calculations

$$\begin{aligned} \sum_n \left[p_n \epsilon_{ijk} x_j \chi_{n,k} + a_n \omega_{n,i} + b_n r^{2n+3} \left(\frac{\omega_n}{r^{2n+1}} \right)_{,i} \right. \\ \left. + c_n \phi_{n,i} + d_n r^{2n+3} \left(\frac{\phi_n}{r^{2n+1}} \right)_{,i} \right] = 0 \end{aligned} \quad (3.32)$$

with

$$\begin{aligned} p_n &= (n-1)\psi_n(\kappa a) + \kappa a \psi'_n(\kappa a) \\ a_n &= \frac{1}{(2n+1)h^2} [\kappa^2 a^2 \psi_n(ha) + 2(n-1)\psi_{n-1}(ha)] \\ b_n &= -\frac{1}{2n+1} \left[\frac{\kappa^2}{h^2} \psi_n(ha) + \frac{2(n+2)}{ha} \psi'_n(ha) \right] \\ c_n &= \kappa^2 a^2 \psi_n(\kappa a) + 2(n-1)\psi_{n-1}(\kappa a) \\ d_n &= \kappa^2 \frac{n}{n+1} \left[\psi_n(\kappa a) + \frac{2(n+2)}{\kappa a} \psi'_n(\kappa a) \right] \end{aligned} \quad (3.33)$$

where we used $\frac{\kappa^2}{h^2} - 2 = \frac{\lambda}{\mu}$.

It is possible to derive a set of equations from (3.32) for $n \neq 0$. The first one is obtained by differentiating with respect to x_i and the second one is obtained by multiplying with x_i . In this way we obtain:

$$\begin{cases} b_n \omega_n + d_n \phi_n = 0 \\ a_n \omega_n + c_n \phi_n = 0 \end{cases} \quad (3.34)$$

There are two separate cases for this set of equations to be considered and therefore the vibrations fall in two classes.

In the first class ω_n and ϕ_n vanish, so we have a unique solution of the set of equations and the determinant of the coefficient matrix is not equal to zero. It follows from (3.32) that for $\omega_n = \phi_n = 0$ the frequency equation is given by:

$$p_n = 0 \quad (3.35)$$

In the second class χ_n vanishes and the determinant is zero. So there is no unique solution and ω_n and ϕ_n are related by the set of equations (3.34). The frequency equation is given by the determinant:

$$b_n c_n - a_n d_n = 0 \quad (3.36)$$

For $n = 0$ the spherical solid harmonics χ_n, ω_n and ϕ_n are constants. Therefore the terms in (3.32) with p_n, a_n and c_n vanish because of the derivative in them. Since the term with p_n disappears from the boundary condition, we have no vibrations of the first class for $n = 0$. The coefficient d_n also vanishes for $n = 0$, so $b_0 = 0$ is the frequency equation for $n = 0$ for the vibrations of the second class.

The numerical evaluation of the equations (3.35) and (3.36) is not trivial. The usual algorithms have different domains for n and the argument of the ψ function where they are stable [5]. As in [5] we have used three different algorithms. The expressions p_n and $b_n c_n - a_n d_n$ are plotted as functions of the frequency for different n in appendix A.

3.4 Vibrations of the first class

These vibrations are also called toroidal modes. The displacement for vibrations of the first class is obtained by substituting $\omega_n = \phi_n = 0$ in (3.30) and restoring the factor $\cos(pt + \epsilon)$:

$$u_i = \cos(pt + \epsilon) \sum_n [\psi_n(\kappa r) \epsilon_{ijk} x_j \chi_{n,k}] \quad (3.37)$$

The frequency equation (3.35) becomes with (3.33)

$$(n - 1)\psi_n(\kappa a) + \kappa a \psi'_n(\kappa a) = 0 \quad (3.38)$$

For fixed n this equation has infinitely many roots. A few of the roots are displayed in figure 3.1 for six values of n .

From (3.22) we see that the dilatation vanishes. Because of the cross product which involves the radius in (3.37) the radial displacement also vanishes. This implies that the sphere only undergoes twistings which keep its volume unchanged. From (3.37) we see that the spherical surfaces determined by $\psi_n(\kappa r) = 0$ are nodal surfaces. The displacement vanishes at these surfaces. It can be shown that a gravitational radiation field has no effect on vibrations of the first class (see [8] and [16]).

If $n = 1$ we have *rotatory vibrations*. This means that all spherical shells concentric with the boundary vibrate round the axis of the shell. Noting that $P_1^0(\cos \theta) = \cos \theta$ we can choose $\chi_1 = r \cos \theta = z$. The displacements (3.37) become:

$$\begin{pmatrix} u_1 \\ u_2 \\ u_3 \end{pmatrix} = \cos(pt + \epsilon) \psi_1(\kappa r) \begin{pmatrix} x_2 \\ -x_1 \\ 0 \end{pmatrix} \quad (3.39)$$

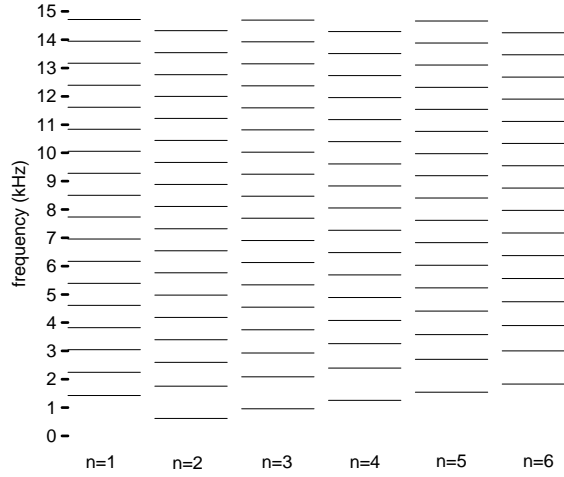


Figure 3.1: The frequency spectrum for vibrations of the first class.

With this choice the spherical surfaces vibrate round the z -axis.

The frequency equation (3.38) turns out to become for $n = 1$

$$\tan(\kappa a) = \frac{3\kappa a}{3 - \kappa^2 a^2} \quad (3.40)$$

The values of κ and a must always satisfy this equation. The function $\tan(\kappa a) - \frac{3\kappa a}{3 - (\kappa a)^2}$ has infinitely many roots for the product κa . This is easy to see because the function behaves as $\tan(\kappa a)$, especially when κa is large. So for a fixed n infinitely many values of κa are allowed and hence infinitely many frequencies.

In figure 3.2 a plot is made for several phases of the vibration. It shows the displacement u_2 on the x_1 axis. u_1 equals zero everywhere because x_2 equals zero on the x_1 axis. So the displayed displacement is the total displacement on this axis. We can see that the amplitude of the vibrations of the spherical shells is the largest near the centre of the sphere. The points on the nodal surfaces are visible.

In figure 3.3 a 3D-plot is made of the displacement in the plane $x_2 = 0$. This plane cuts the vibrating spherical shells in two equal parts. The displacement vanishes on the x_3 -axis.

3.5 Vibrations of the second class

This class of vibrations is also referred to as spheroidal modes. Radial as well as tangential displacements take place. The displacement is obtained by substituting $\chi_n = 0$ in (3.30), setting $n = n - 1$ in the last two terms and restoring the phase factor:

$$u_i = \cos(pt + \epsilon) \sum_n \left[-\frac{1}{h^2} [\omega_n \psi_n(hr)]_{,i} + \psi_{n-1}(kr) \phi_{n,i} - \frac{n}{n+1} \psi_{n+1}(\kappa r) \kappa^2 r^{2n+3} \left(\frac{\phi_n}{r^{2n+1}} \right)_{,i} \right] \quad (3.41)$$

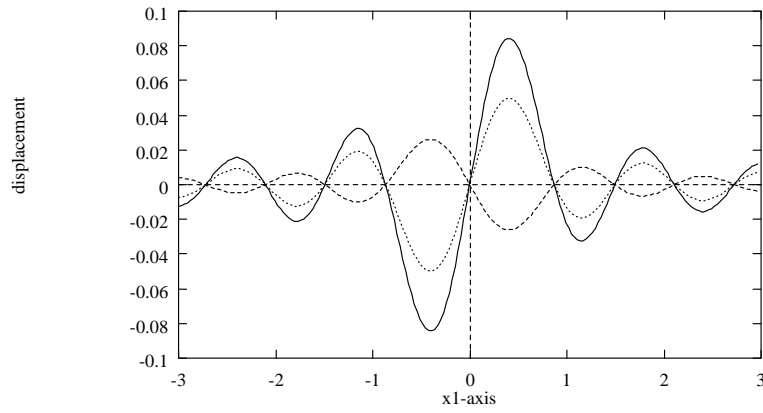


Figure 3.2: Rotatory vibrations for $n = 1$. The displacement in the x_2 direction is shown along the x_1 -axis in the plane $x_3 = 0$. We took $\kappa = 5.17$ (corresponding to a frequency of 1914 Hz) and $a = 3$ m.

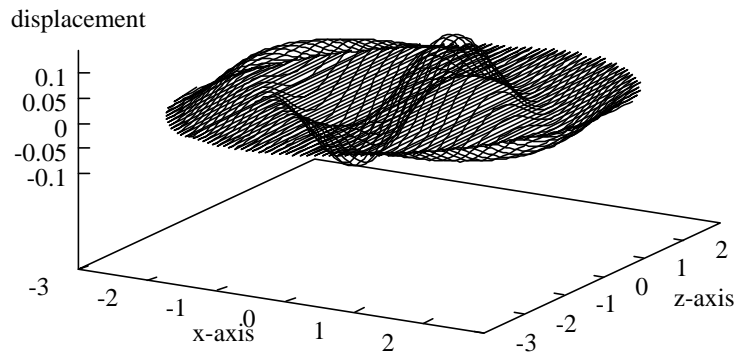


Figure 3.3: Rotatory vibrations for $n = 1$. The displacement on a cross section of the spherical shells rotating round the z -axis. We took $\kappa = 3.03$ (corresponding to a frequency of 1122 Hz) and $a = 3$ m.

Some of the solutions of the frequency equation (3.36) are displayed in figure 3.4.

The next chapter is devoted to this class of vibrations for $n = 2$. In this case the modes are called quadrupole modes. These modes couple to the gravitational radiation field [8].

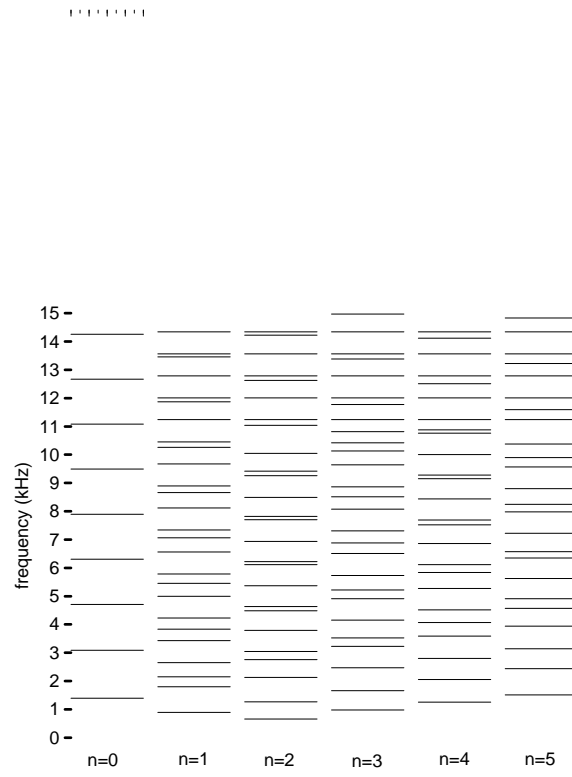


Figure 3.4: The frequency spectrum for vibrations of the second class.

Chapter 4

Quadrupole modes

In this chapter we consider a special case of the solutions found in the previous one. For $n = 2$ the vibrations of the second class are called quadrupole modes. Our main attention goes to these modes because they interact with the gravitational radiation field [16].

4.1 Frequencies of the quadrupole modes

There are several frequencies which satisfy (3.36) for $n = 2$. When the numerical values of the Lamé constants are known we can eliminate either h or κ from (3.36) and our other equations. Therefore we recall the definitions:

$$h^2 = \frac{p^2 \rho}{\lambda + 2\mu}$$

$$\kappa^2 = \frac{p^2 \rho}{\mu}$$

With the values for copper from table 2.1 we find $\lambda \cong 2.19\mu$ and $h \cong \frac{\kappa}{2.05}$. With this we eliminate h from the frequency equation in favour of κ . Note that κ is a measure for the frequency f because it equals a constant only depending on the material times the frequency:

$$f = \frac{1}{2\pi} \sqrt{\frac{\mu}{\rho}} \kappa \quad (4.1)$$

We denote the frequencies in ascending order by $\kappa_1, \kappa_2, \kappa_3, \dots$. The lowest root κ_1 corresponds to a frequency of $f = 654.083$ Hz.

4.2 Expressions for the displacements

For $n = 2$ there are five values of m allowed. For $m \neq 0$ the surface harmonics become complex functions. To obtain real valued displacements we define real quadrupole spherical harmonics as in [16]:

$$Y_0 \equiv Y_2^0 = \sqrt{\frac{5}{16\pi}} \left(3 \frac{z^2}{r^2} - 1 \right)$$

$$\begin{aligned}
Y_{1c} &\equiv \frac{1}{\sqrt{2}}(Y_2^{-1} - Y_2^{+1}) = \sqrt{\frac{15}{4\pi}} \left(\frac{xz}{r^2} \right) \\
Y_{1s} &\equiv \frac{i}{\sqrt{2}}(Y_2^{-1} + Y_2^{+1}) = \sqrt{\frac{15}{4\pi}} \left(\frac{yz}{r^2} \right) \\
Y_{2c} &\equiv \frac{1}{\sqrt{2}}(Y_2^{-2} + Y_2^{+2}) = \sqrt{\frac{15}{16\pi}} \left(\frac{x^2 - y^2}{r^2} \right) \\
Y_{2s} &\equiv \frac{i}{\sqrt{2}}(Y_2^{-2} - Y_2^{+2}) = \sqrt{\frac{15}{4\pi}} \left(\frac{xy}{r^2} \right)
\end{aligned} \tag{4.2}$$

According to [16] and [10] the displacements that are obtained by using these real spherical harmonics can be written as follows:

$$\mathbf{u}_l = [a(h, \kappa, r)\hat{\mathbf{r}} + b(h, \kappa, r)\nabla]Y_l \tag{4.3}$$

Here l denotes one of the modes (0, 1c, 1s, 2c, 2s) and $\hat{\mathbf{r}}$ is the unit normal in the direction of r . The functions $a(h, \kappa, r)$ and $b(h, \kappa, r)$ determine the motion in the radial and tangential direction, respectively. We are able to obtain expressions for these functions by substituting $\omega_2 = \phi_2 = r^2 Y_l, l = 0, 1c, 1s, 2c, 2s$ in (3.41). In this way we can deduce

$$a(h, \kappa, r) = -\frac{1}{h^4} \frac{\partial}{\partial r} j_2(hr) - \frac{10}{\kappa^2 r} j_2(\kappa r) \tag{4.4}$$

and

$$b(h, \kappa, r) = -\frac{1}{h^4} j_2(hr) - \frac{5}{3\kappa^2} \frac{\partial}{\partial r} [r j_2(\kappa r)] \tag{4.5}$$

j_2 is the spherical Bessel function of the second order. With these forms for $a(h, \kappa, r)$ and $b(h, \kappa, r)$ the displacements (4.3) are in correspondence with the ones deduced in [2]. The functions are shown in figures 4.1 and 4.2 for several frequencies.

As is to be seen from the expressions for the real spherical quadrupole harmonics, the modes 1c, 1s and 2s have the same shape. This should be clear because the real spherical quadrupole harmonics have the same form. The only difference is that other coordinates appear in them. So the modes have the same shape but a different orientation. It turns out that the Y_{2c} mode also has the same shape as these three modes. This is due to the fact that Y_{2c} is equal to Y_{2s} under a rotation of 45 degrees in the xy -plane. This is shown as follows. Consider a rotation of the coordinate system about an angle α as shown in figure 4.3. The point P at distance r from the origin has the coordinates $x = r \cos \gamma$ and $y = r \sin \gamma$ in the old coordinate system. In the new coordinate system the coordinates become:

$$\begin{aligned}
x' &= r \cos \beta = r \cos(\gamma - \alpha) = r \cos \gamma \cos \alpha + r \sin \gamma \sin \alpha = x \cos \alpha + y \sin \alpha \\
y' &= r \sin \beta = r \sin(\gamma - \alpha) = r \sin \gamma \cos \alpha - r \cos \gamma \sin \alpha = y \cos \alpha - x \sin \alpha
\end{aligned}$$

By using this coordinate transformation with $\alpha = \frac{1}{4}\pi$ and denoting the rotated system with an accent we can write

$$(Y_{2c})' = \sqrt{\frac{15}{16\pi}} \left(\frac{x'^2 - y'^2}{r^2} \right) = \sqrt{\frac{15}{4\pi}} \left(\frac{xy}{r^2} \right) = Y_{2s} \tag{4.6}$$

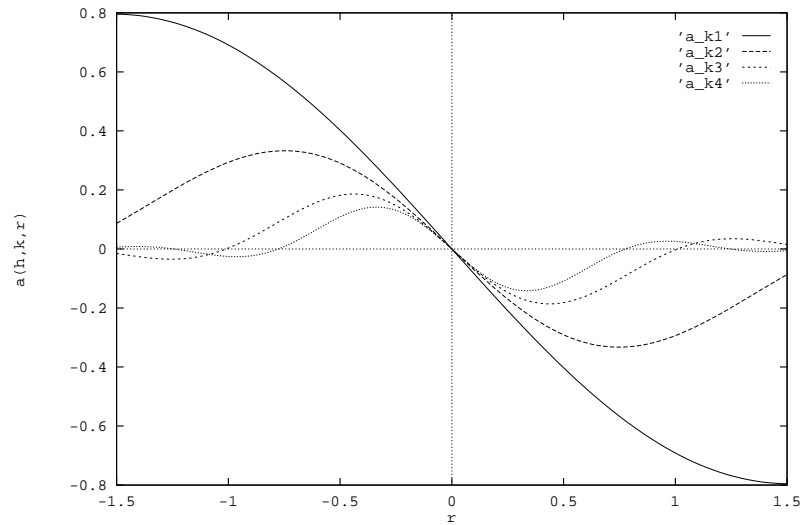


Figure 4.1: Spheroidal vibrations. $n=2$. The function $a(h, \kappa, r)$ appearing in the solution for several frequencies.

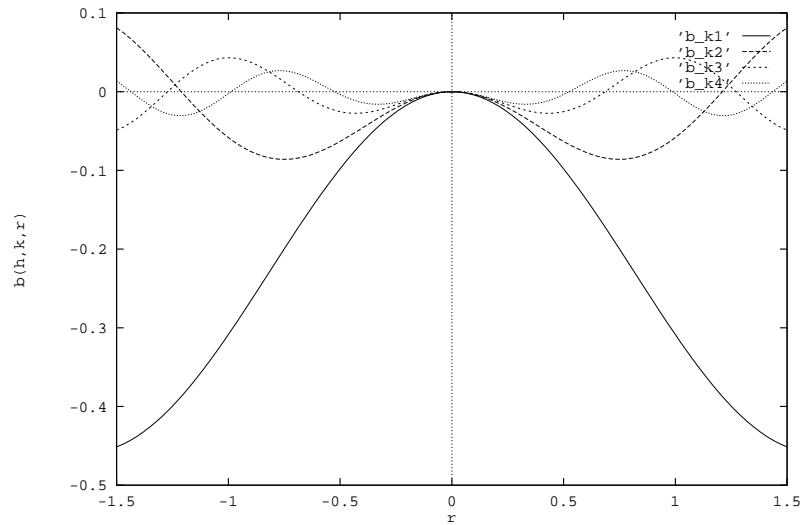


Figure 4.2: Spheroidal vibrations. $n=2$. The function $b(h, k, r)$ appearing in the solution for several frequencies.

So the orientation of the $2c$ and $2s$ modes differs a rotation of $\frac{1}{4}\pi$ about the z -axis. It should be clear that the orientation of the $1c$ and $1s$ modes also differ a rotation about the z -axis. In this latter case we have $\alpha = \frac{1}{2}\pi$.

The $l = 0$ mode is a superposition of two of the other modes which are rotated. We denote a rotation in the xz -plane with a double accent and a rotation in the yz -plane with

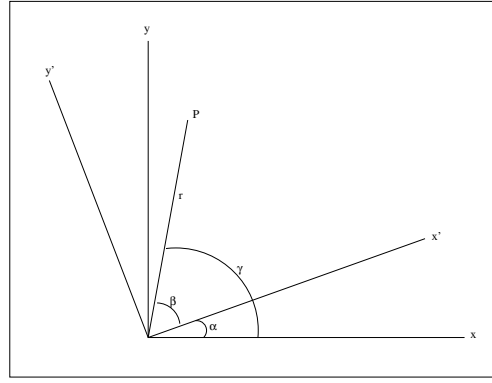


Figure 4.3: The coordinate system built by the axes x and y is rotated about an angle α . The new system consists of the x' and the y' axes. The point P at distance r from the origin has coordinates $x = r \cos \gamma$ and $y = r \sin \gamma$ in the old system. In the new system the coordinates are $x' = r \cos \beta$ and $y' = r \sin \beta$.

a triple accent. If we rotate about an angle of $-\frac{1}{4}\pi$ we get

$$(Y_{1c})'' = \sqrt{\frac{15}{4\pi}} \left(\frac{x'' z''}{r^2} \right) = \sqrt{\frac{15}{16\pi}} \left(\frac{z^2 - x^2}{r^2} \right) \quad (4.7)$$

and

$$(Y_{1s})''' = \sqrt{\frac{15}{4\pi}} \left(\frac{y''' z'''}{r^2} \right) = \sqrt{\frac{15}{16\pi}} \left(\frac{z^2 - y^2}{r^2} \right) \quad (4.8)$$

Addition of (4.7) and (4.8) gives Y_0 , except for a factor $\sqrt{3}$.

So the real quadrupole spherical harmonics (4.2) can only transform into each other by using a rotation. Our conclusion is that they form an independent basis for all the quadrupole vibrations.

4.3 Visualization of the modes

The modes are displayed in figures 4.4, 4.6 and 4.5.

The $l = 0$ mode is displayed in figure 4.4. The sphere is consecutively distorted into a prolate and an oblate spheroid. A spheroid is an ellipsoid for which two of the three semi-axes have equal length. For a prolate spheroid these two axes are shorter than the third one, it resembles a cigar. This body can be made by revolving an ellipse about its long axis. In the case of an oblate ellipsoid, the two semi-axes that have equal length are longer than the third one. If the difference in length becomes large, the oblate ellipsoid comes to look like a pancake. The shape may be obtained by revolving an ellipse about its short axis.

In the other four modes the sphere alternates between two mutually perpendicular oblate ellipsoids. In the $2c$ -mode (figure 4.5) the sphere distorts from an oblate form in which it is stretched in the y -direction and flat in the x -direction into an oblate form in which it is stretched in the x -direction and flat in the y -direction. One of the other three modes in which the sphere alternates between two oblate forms is displayed in figure 4.6. The oblate

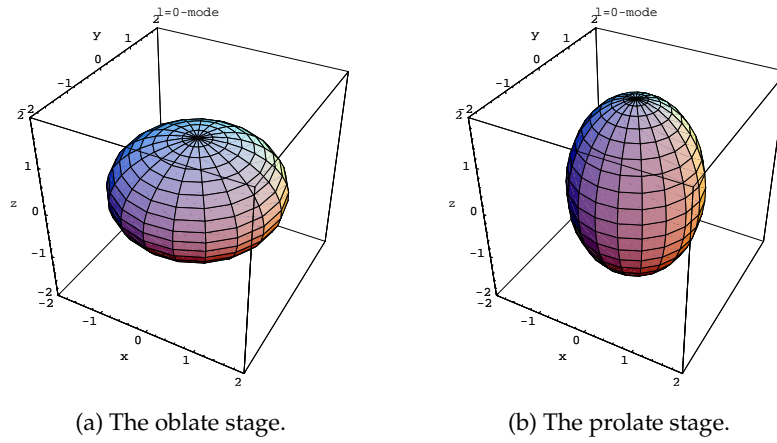


Figure 4.4: The $l = 0$ quadrupole mode displayed at two stages of the vibration. The stages differ half a period.

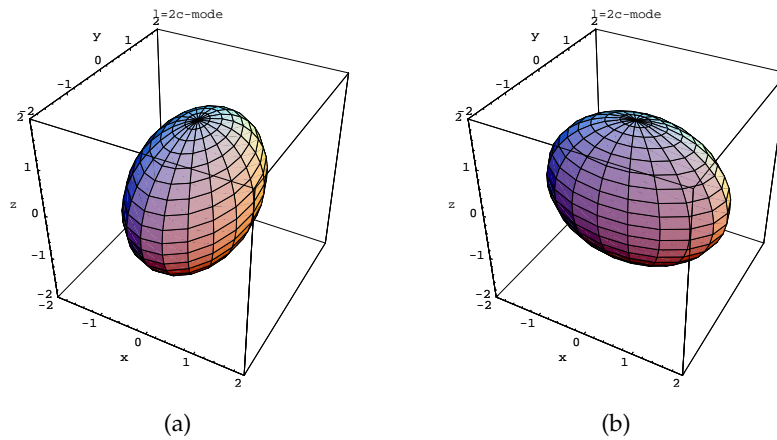


Figure 4.5: The $l = 2c$ quadrupole mode at two stages of the vibration. The stages differ half a period. The sphere is distorted into an oblate ellipsoid in both the figures (a) and (b).

forms are not clear from this figure because we look at the flat side of the oblate ellipsoid in figure (a) as well as in (b). The displacement in one coordinate direction vanishes for these four oblate-oblate modes.

The displacements along the three planes which divide the sphere in two equal parts are shown in figure 4.7 for $l = 0$ for the lowest frequency. We see that the sphere is stretched along two axes (the x - and y -axis) and shortened along one axis (the z -axis) at this stage of the motion. This corresponds to figure 4.4(a).

These displacements are shown for the $2c$ mode in figure 4.8. This configuration corresponds to figure 4.5(a).

For the second lowest frequency the displacements are shown in figures 4.9 for the $l = 0$ mode. Again the displacement in the yz -plane gives the same picture as the displacement

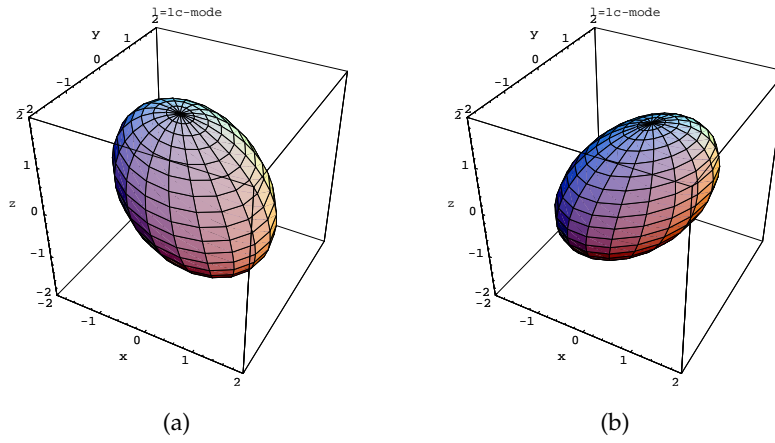


Figure 4.6: The $l = 1c$ quadrupole mode at two stages of the vibration. The stages differ half a period.

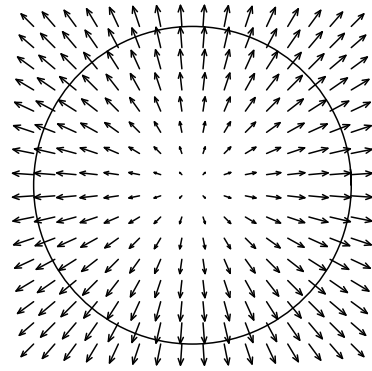
in the xz -plane. If we compare figure 4.7(a) with figure 4.9(a) we see that the displacements are larger when the points are further away from the centre of the sphere in the first picture. This is not the case in the second figure which corresponds to a higher frequency. We can conclude that the higher the frequency, the more compressions and stretches we get in the sphere. This fact can also be deduced from figures 4.1 and 4.2. The higher the frequency, the more complex the functions $a(h, \kappa, r)$ and $b(h, \kappa, r)$ become.

Notice that the displacement almost vanishes near the surface of the sphere in figure 4.9. This indicates that these vibrations will be difficult to measure.

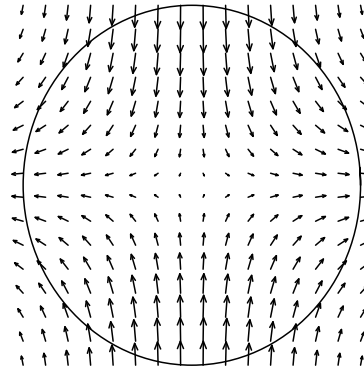
4.4 Deviations of the frequency

The frequencies of the normal modes are influenced by the following parameters.

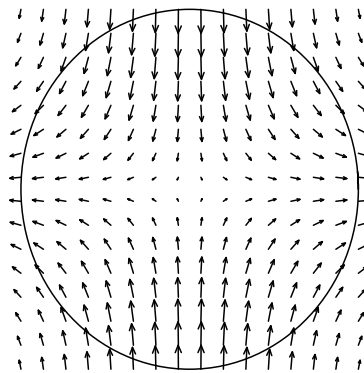
- The **Poisson ratio** σ . For copper we have $\sigma = 0.343$. Now we vary this ratio in the range from table 2.1 to see how it affects the normal mode frequencies. This is shown in figure 4.10(a) for the lowest root and in figure 4.10(b) for the second root. It is remarkable that in the first case the frequency decreases when the Poisson ratio is increased, while in the second case the frequency increases with the Poisson ratio.
- The **Young's modulus** E . In figures 4.11(a) and 4.11(b) we see how the frequency depends on the Young's modulus. Because we have varied the Poisson ratio and the Young's modulus both between the extreme values of real materials from table 2.1, we can say that the sensitivity of the frequency to the Young's modulus is much larger than to the Poisson ratio.
- The **radius** of the sphere. The dependence of the two lowest roots κ_1 and κ_2 of (3.36) on the radius of the sphere is shown in figures 4.12(a) and 4.12(b). As was to be expected the curves in these figures are part of the hyperbola $\kappa a = \text{constant}$.



(a) Displacement in the xy -plane.

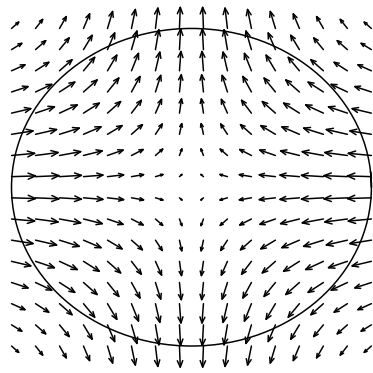


(b) Displacement in the xz -plane.

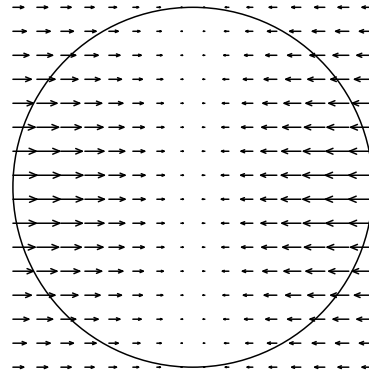


(c) Displacement in the yz -plane

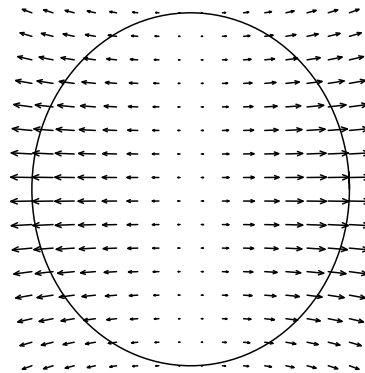
Figure 4.7: The $l = 0$ quadrupole mode. Displacement in three planes through the sphere for the lowest frequency.



(a) Displacement in the xy -plane.



(b) Displacement in the xz -plane.



(c) Displacement in the yz -plane

Figure 4.8: The $l = 2c$ quadrupole mode. Displacement in three planes through the sphere for the lowest frequency.

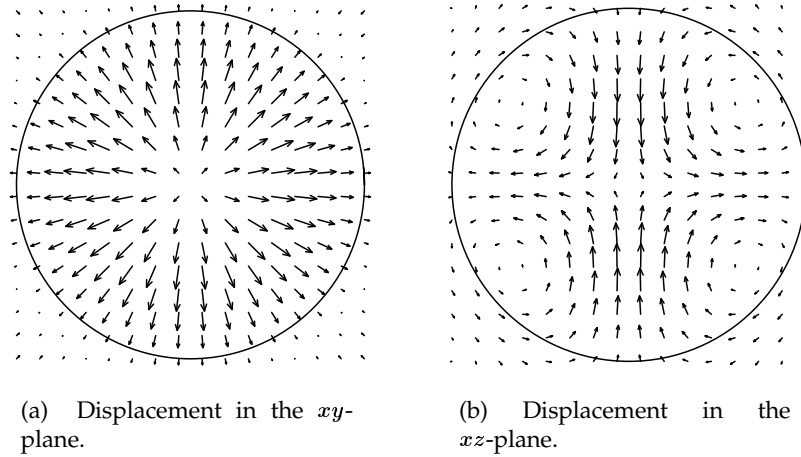


Figure 4.9: The $l = 0$ quadrupole mode. Displacement in two planes through the sphere for the second lowest frequency.

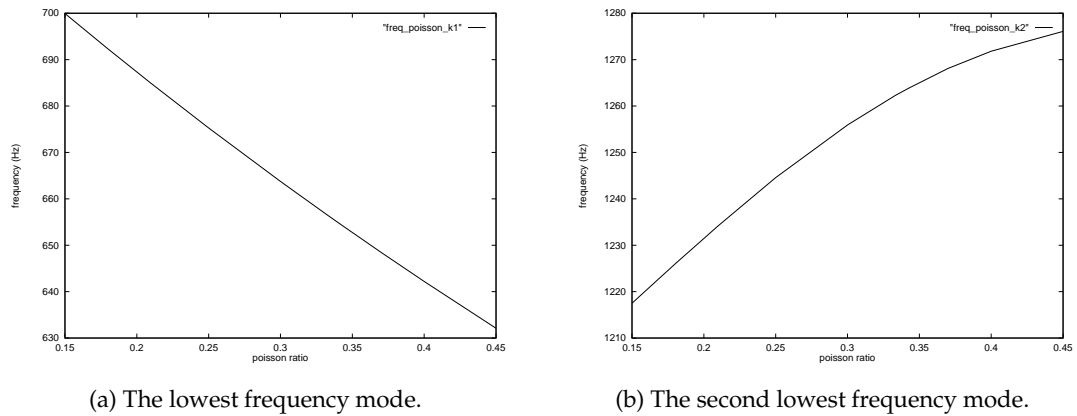
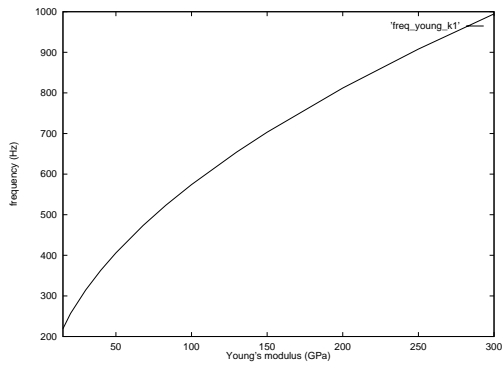
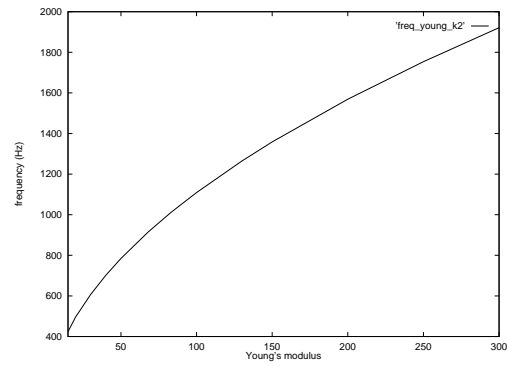


Figure 4.10: Quadrupole modes. The frequency is plotted against the Poisson ratio. The radius and the Young's modulus are kept constant here at $a = 1.5$ m and $E = 129.8$ GPa.

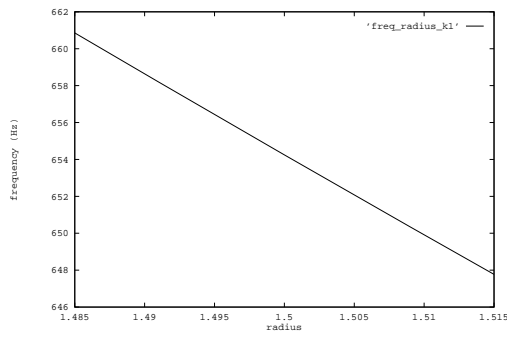


(a) The lowest frequency mode.

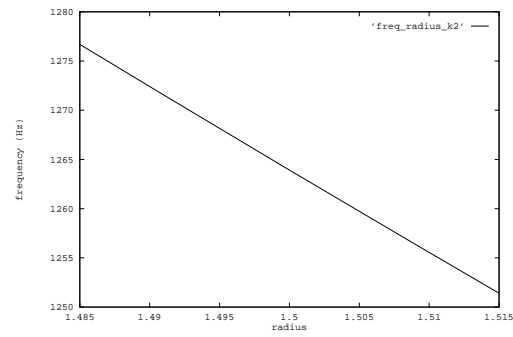


(b) The second lowest frequency mode.

Figure 4.11: Quadrupole modes. The frequency is plotted against the Young's modulus. The radius and the Poisson ratio are kept constant here at $a = 1.5$ m and $\sigma = 0.343$.



(a) The lowest frequency mode.



(b) The second lowest frequency mode.

Figure 4.12: Quadrupole modes. The frequency is plotted against the radius of the sphere. The Poisson ratio $\sigma = 0.343$ m and Young's modulus $E = 129.8$ GPa are held constant here.

Part III

Variational Methods

Chapter 5

A variational approach to approximate the normal modes of elastic objects

As we have seen in the previous chapter the exact solutions to the differential equations are quite complex, even in the case of a perfect homogeneous isotropic sphere. It is impossible to solve them in general. Approximation procedures have been developed for this reason. We will use an approach that is based on the variational principle, i.e. the stationarity of the Lagrangian of the system in question, see [3] and [4]. The displacement functions will be expanded into a truncated complete set of functions. The coefficients of the expansion will be approximated numerically with the aid of the variational principle. As a basis we will choose the functions proposed in [15].

5.1 Hamilton's principle applied to elasticity theory

The theoretical background for the numerical approximation procedure is described in this section.

In the theory of Hamilton we have a quantity called the Lagrangian. In general the Lagrangian L can be formed by subtracting the potential energy density from the kinetic energy density and integrating over the space occupied by the object under consideration:

$$L = \int_{\tau} (T - V) d\tau \quad (5.1)$$

In elasticity theory we take $T = \frac{1}{2}\rho p^2 u_i u_i$ and $V = \frac{1}{2}c_{ijkl} u_{i,j} u_{k,l}$. As before ρ is the density, p the angular frequency, c_{ijkl} the elastic tensor appearing in (2.22) and u_i the displacement field. In this way we obtain

$$L = \int_{\tau} \left(\frac{1}{2}\rho p^2 u_i u_i - \frac{1}{2}c_{ijkl} u_{i,j} u_{k,l} \right) d\tau \quad (5.2)$$

We will now show that the equations that describe free vibration of an elastic solid, with c_{ijkl} independent of the position, naturally follow from demanding stationarity of the Lagrangian. This is the variational principle. We want to know what the variation in L is

when we vary u_i by δu_i . To deduce this we replace u_i in (5.2) by $u_i + \delta u_i$ and neglect terms of order $(\delta u_i)^2$. In this way we obtain:

$$L + \delta L = \int_{\tau} \left(\frac{1}{2} \rho p^2 (u_i u_i + 2u_i \delta u_i) - \frac{1}{2} c_{ijkl} (u_{i,j} u_{k,l} + u_{k,l} \delta u_{i,j} + u_{i,j} \delta u_{k,l}) \right) d\tau \quad (5.3)$$

In this expression we can recognize the form for L given in (5.2). When we subtract (5.2) from (5.3) and note that we can write $\frac{1}{2} c_{ijkl} (u_{k,l} \delta u_{i,j} + u_{i,j} \delta u_{k,l}) = c_{ijkl} u_{k,l} \delta u_{i,j}$ because of the property $c_{ijkl} = c_{klij}$ we obtain:

$$\delta L = \int_{\tau} (\rho p^2 u_i \delta u_i - c_{ijkl} u_{k,l} \delta u_{i,j}) d\tau \quad (5.4)$$

After performing a partial integration we arrive at

$$\delta L = \int_{\tau} (\rho p^2 u_i \delta u_i + \delta u_i [c_{ijkl} u_{k,l}]_{,j} - [c_{ijkl} u_{k,l} \delta u_i]_{,j}) d\tau \quad (5.5)$$

Now we use the Gauss theorem to rewrite the last term in the volume integral into a surface integral.

$$\delta L = \int_{\tau} (\rho p^2 u_i + c_{ijkl} u_{k,l,j}) \delta u_i d\tau - \int_{\sigma} (\nu_j c_{ijkl} u_{k,l}) \delta u_i d\sigma \quad (5.6)$$

ν_j is the component in the direction of the x_j -axis of the outward pointing unit normal on the surface of the object. In the last step we also used $c_{ijkl,j} = 0$. The expression between brackets in the integrand of the surface integral is just the surface traction. This expression is to be compared with the one in the upper line of (3.31) for a sphere. If we replace in the case of the sphere x_j/r by ν_j and note that $\tau_{ij} = c_{ijkl} e_{kl} = c_{ijkl} u_{k,l}$ we obtain the more general form for the surface traction given above. For a freely vibrating object the surface traction equals zero. The volume integral also equals zero because the elastic wave equation appears between the brackets. Now we have deduced that for a free vibrating elastic object with c_{ijkl} independent of position we have $\delta L = 0$. We are going to use this fact in the following.

5.2 Numerical algorithm

We expand the displacements in a set of basis functions. There are several possibilities for the choice of these functions. See for example [3] and [4]. In [15] the displacement vector is expanded in the simplest possible set of functions. These functions are the products of non-negative integer powers of the Cartesian coordinates:

$$\Phi_{\lambda} = x^l y^m z^n \quad (5.7)$$

λ represents a set of three non-negative integers (l, m, n) . Later on we will see that it is a convenient choice to take these simple functions, because their products will serve as integrand in a volume integral. We will use these basis functions because many different shapes can be studied with this choice of functions. The displacements can be written as

$$u_i = \sum_{\lambda \in \Omega} a_{\lambda i} \Phi_{\lambda} \quad (5.8)$$

The $a_{\lambda i}$ are the coefficients to be determined. Ω defines a truncation of the set. For absolute representation Ω should be the set in which l, m and $n \in \mathbb{N}$. Since we can not compute infinitely many coefficients we have to truncate the set. For some N this truncation is specified by

$$l + m + n \leq N \quad (5.9)$$

We hope that our approximation will be good enough.

Now we substitute (5.8) in (5.2) and replace all the summations by a convenient matrix notation:

$$L = \frac{1}{2} p^2 \mathbf{a}^T E \mathbf{a} - \frac{1}{2} \mathbf{a}^T \Gamma \mathbf{a} \quad (5.10)$$

The coefficients $a_{\lambda i}$ have been placed in a column vector \mathbf{a} . The two matrices E and Γ are given by:

$$E_{\lambda i \lambda' i'} = \delta_{ii'} \rho \int_{\tau} \Phi_{\lambda} \Phi_{\lambda'} d\tau \quad (5.11)$$

$$\Gamma_{\lambda i \lambda' i'} = c_{ijj'j'} \int_{\tau} \Phi_{\lambda, j} \Phi_{\lambda', j'} d\tau \quad (5.12)$$

Note that the length of the vectors, the number of columns and the number of rows of the matrices are all equal to three (three coordinate directions) times the number of functions Φ_{λ} used. So the size of the matrices and vectors grows fast when N is increased. The size of the matrices denoted by $R \times R$ is related to N according to

$$R = \frac{1}{2}(N + 1)(N + 2)(N + 3)$$

The fact $\delta L = 0$ indicates that we must set all the derivatives of (5.10) with respect to the indices $a_{\lambda i}$ equal to zero. This renders the following matrix eigenvalue equation:

$$p^2 E \mathbf{a} = \Gamma \mathbf{a} \quad (5.13)$$

This generalized eigenvalue problem is implemented in a computer program. By solving the problem we get to know the frequencies p of the normal modes and the coefficients $a_{\lambda i}$. With these coefficients we can also determine the shape of the modes with the aid of (5.8). In our implementation a LAPACK [1] routine is used.

We can take advantage of the simple form of our basis functions when we have to calculate the matrix elements from formulas (5.11) and (5.12). The integrands have the same form as the basis functions and the integrals can be evaluated analytically for many shapes:

$$\int_{\tau} x^p y^q z^r d\tau = f(p, q, r) \quad (5.14)$$

Objects for which such a $f(p, q, r)$ can be found are spheres, hemispheres, ellipsoids, cylinders, cones, pyramids, parallelepipeds and many others.

The c_{ijkl} appearing in (5.12) depend on the Lamé parameters λ and μ in the following way: $c_{ijkl} = \lambda + 2\mu$ when all the indices are equal, $c_{ijkl} = \lambda$ when $i = j$ and $k = l$ and $c_{ijkl} = \mu$ when $i = k$ and $j = l$. In this last case the following symmetry properties of the elastic tensor must be used: $c_{ijkl} = c_{jikl} = c_{ijlk}$

Chapter 6

Applications of the approximation method

We will apply the variational method from the previous chapter here. First we will regard the results for a solid sphere. In this way we can compare the approximation method with the analytical one. Furthermore we will apply it to prolate and oblate spheroids, a sphere with a concentric hole and a sphere with a bore hole.

6.1 A solid sphere

For a sphere with radius a centered at the origin we have an analytical solution for the integrals (5.11) and (5.12):

$$\begin{aligned} \int_{\tau} x^p y^q z^r d\tau &= \int_{z=-a}^a \int_{y=-\sqrt{a^2-z^2}}^{\sqrt{a^2-z^2}} \int_{x=-\sqrt{a^2-y^2-z^2}}^{\sqrt{a^2-y^2-z^2}} x^p y^q z^r dx dy dz \\ &= \frac{4a^{3+p+q+r} \Gamma_{\frac{1}{2}}(3+p) \Gamma_{\frac{1}{2}}(1+q)}{(1+p)(2+p+q)} \left[\frac{\Gamma_{\frac{1}{2}}(1+r)}{\Gamma_{\frac{1}{2}}(3+p+q+r)} - \frac{\Gamma_{\frac{1}{2}}(3+r)}{\Gamma_{\frac{1}{2}}(5+p+q+r)} \right] \\ &= \frac{4\pi a^{3+p+q+r} (p-1)!! (q-1)!! (r-1)!!}{(3+p+q+r)!!} \end{aligned} \quad (6.1)$$

Γ_n is the Euler Gamma function and the double factorial is defined as $n!! = 1 \cdot 3 \cdot 5 \cdot \dots \cdot n$, with $(0)!! = (-1)!! = 1$. The last step from (6.1) can be verified by using the relation:

$$\Gamma_{n+\frac{1}{2}} = \frac{(2n-1)!!}{2^n} \Gamma_{\frac{1}{2}} = \frac{(2n-1)!!}{2^n} \sqrt{\pi} \quad (6.2)$$

It should be noticed that the integral (6.1) vanishes when one or more of the p , q or r are odd. This is due to the facts that in this case the integrand becomes an odd function of the coordinate pertinent to the odd power and that the sphere is symmetric with respect to the origin. Hence the whole integral vanishes when the integration over a coordinate with an odd power is performed.

In table 6.1 the results of the program are compared with the analytical solutions from chapter 3 for the frequency range of our interest. The values converge well to the analytical

n	cl.	analytical solution	$N = 5$ $R = 168$	$N = 6$ $R = 252$	$N = 7$ $R = 360$	$N = 8$ $R = 495$	$N = 9$ $R = 660$	$N = 10$ $R = 858$
2	1	617.0786	617.183	617.079	617.079	617.079	617.079	617.079
2	2	654.0828	654.090	654.090	654.085	654.085	654.085	654.085
1	2	891.7504	893.488	891.796	891.796	891.788	891.788	891.788
3	1	953.4975	954.323	954.323	953.500	953.500	953.500	953.500
3	2	975.4565	988.374	975.550	975.550	975.464	975.464	975.464
4	2	1251.997	-	1281.98	1252.35	1252.35	1252.01	1252.01
4	1	1256.942	-	1259.45	1259.45	1256.96	1256.96	1256.94
2	2	1263.632	1270.78	1270.78	1263.78	1263.78	1263.68	1263.68
0	2	1395.698	1396.06	1396.06	1396.06	1396.06	1396.06	1396.06
1	1	1421.959	1444.79	1444.79	1422.48	1422.48	1421.96	1421.96
5	2	1510.716	-	-	-	1511.6	1511.65	1510.83
5	1	1545.889	-	1561.22	1551.12	1551.12	1545.95	1545.95
3	2	1661.032	-	1681.20	1681.20	1661.6	1661.63	1661.04
6	2	1760.268	-	-	-	-	1762.42	1762.42
2	1	1760.594	-	1808.6	1808.6	1762.4	1762.43	1760.62
1	2	1793.638	-	1843.70	1843.70	1795.91	1795.81	1793.67

Table 6.1: The analytical and the calculated frequencies in Hz for a few modes of a sphere.

solution for most of the modes. The modes in the table are the only ones with a frequency in this range. R stands for the size of the matrices. It is indicated whether a mode falls in the first or in the second class in the column "cl.". These two classes are discussed in chapter 3.

There are two ways to distinguish the modes. First we can look at the degeneracy. The program gives each eigenvalue $2n + 1$ times. In the second place we can make vector plots like the ones in figure 4.7. The first six eigenvalues are always equal to zero. These values correspond to three rotations and three translations. A dash is given in the table if a mode is not yet found. The higher N , the more frequencies of modes with higher n are found. This is caused by the fact that the modes with higher n have more nodal points and the expansion also gets more roots when N gets higher. Higher modes need higher N for reasonable representation.

6.2 Prolate and oblate spheroids

We have varied the length of one axis to see how this influences the normal modes of the resulting spheroids. In general an ellipsoid is described by its three semi-axes d_x , d_y and d_z :

$$\frac{x^2}{d_x^2} + \frac{y^2}{d_y^2} + \frac{z^2}{d_z^2} = 1 \quad (6.3)$$

For a sphere these axes have equal length. When we make one semi-axis longer and keep the other two constant at 1.5 m the object is called a prolate spheroid. If we make one semi-axis shorter than the other two we have an oblate spheroid. For an ellipsoid the integral

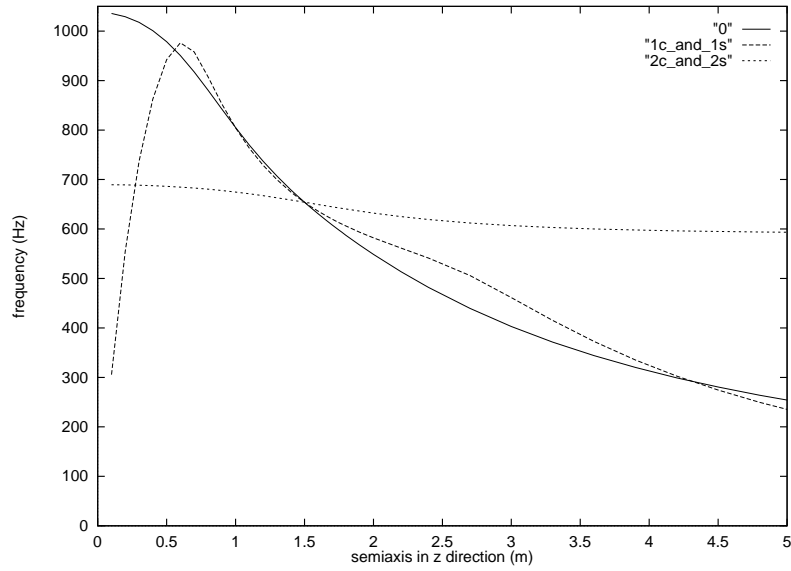


Figure 6.1: The vibrations of spheroids are considered. To do so, one of the semi-axes of a sphere is varied, while the other two are kept constant at 1.5 m. The Lamé parameters for copper are used. The quadrupole modes with the lowest frequencies are displayed. The calculations are performed with $N = 6$.

(6.1) becomes:

$$\begin{aligned}
 \int_{\tau} x^p y^q z^r d\tau &= 8 \int_{z=0}^{d_z} \int_{y=0}^{\sqrt{d_y^2 \left(1 - \frac{z^2}{d_z^2}\right)}} \int_{x=0}^{\sqrt{d_x^2 \left(1 - \frac{y^2}{d_y^2} - \frac{z^2}{d_z^2}\right)}} x^p y^q z^r dx dy dz \\
 &= \frac{4\pi d_x^{p+1} d_y^{q+1} d_z^{r+1} (p-1)!! (q-1)!! (r-1)!!}{(3+p+q+r)!!}
 \end{aligned} \tag{6.4}$$

Again we have the restriction that the integral vanishes when one or more of the p , q or r are odd.

In figure 6.1 d_z is varied from 0.1 m to 5.0 m. We can see that the degeneracy is partially removed because the five modes have three different frequencies now. The $l = 0$ mode gets a unique frequency. The four oblate-oblate modes get two different frequencies. The $2c$ and $2s$ modes, which have no displacement in the z direction, get the same frequency. Their orientation with respect to the z -axis and hence with respect to the shape of the object is the same. The $1c$ and $1s$ modes do have a displacement in the z direction. These two modes also have the same orientation with respect to the shape of the object. So they keep the same frequency when we make a spheroid out of the sphere also.

When we take another semi-axis to vary we get the same figure. The computer program always "fits" the $l = 0$ mode onto the shape of the object. For a prolate spheroid, the prolate form of the $l = 0$ mode lines up with the prolate form of the object. For an oblate spheroid the two oblate forms line up. The other modes rotate accordingly, so we maintain an independent basis. In [11] it is also found that the asymmetry fixes the spatial orientation of the quadrupole eigenfunctions.

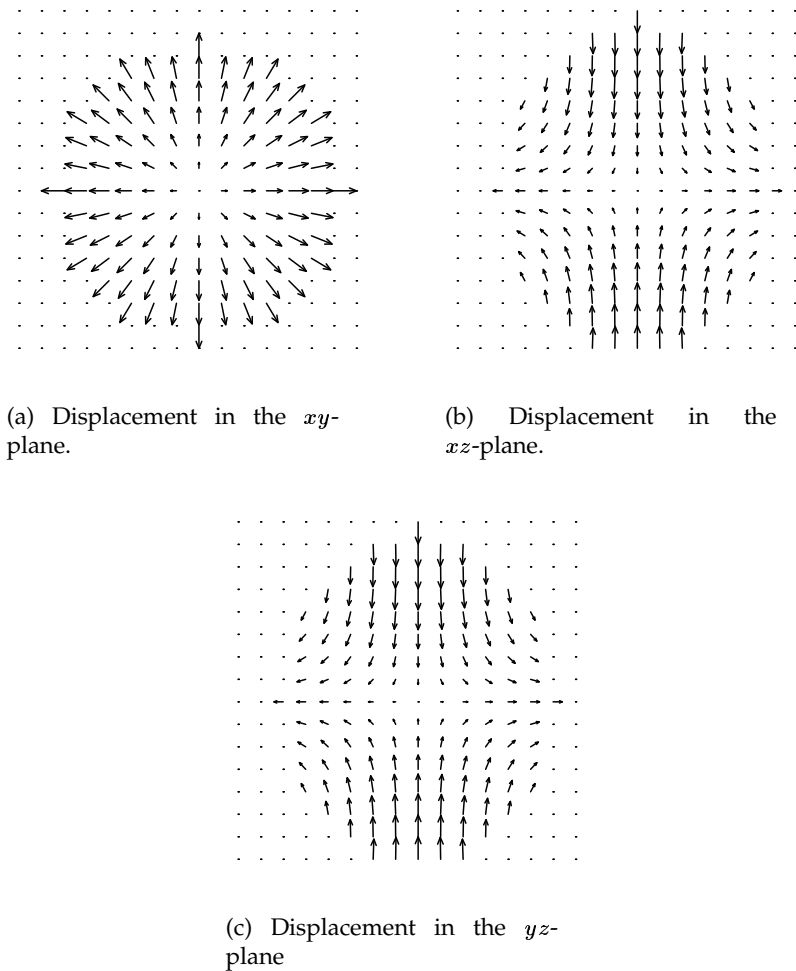


Figure 6.2: The $l = 0$ quadrupole mode. Displacement in three planes through a prolate spheroid for the lowest frequency. $d_z = 2$ m, $d_x = 1.5$ m and $d_y = 1.5$ m.

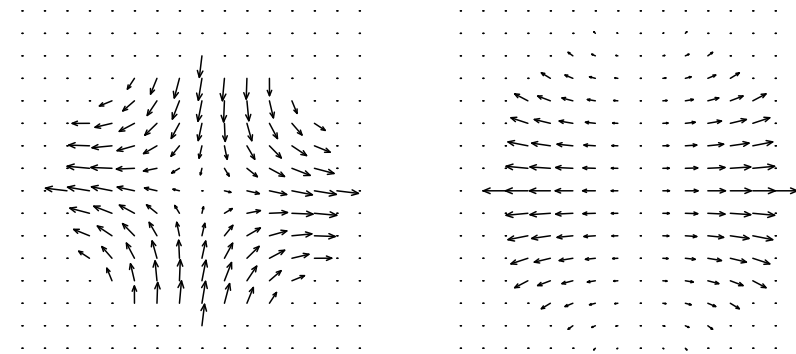
The displacements in three planes through the spheroid are shown in figure 6.2 for the $l = 0$ mode and in figure 6.3 for the $l = 2c$ mode.

In table 6.2 the calculated frequencies are shown for the different modes at different values of d_z and for increasing N . We see that a significant loss in efficiency of our approximation method only occurs in the $2c$ and $2s$ modes for $N = 6$ when we stretch the sphere.

6.3 A concentric hole

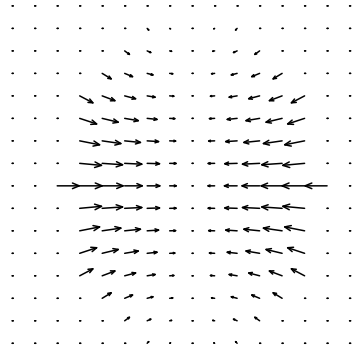
The spherical shape is perturbed by making a concentric hole in the middle now. The outer and inner radii are denoted by a and b , as is indicated in figure 6.4(a).

Formula (6.1) has to be modified in a simple way to implement this concentric sphere in a computer program. We can just subtract from (6.1) a term of the same form with a substituted by b .



(a) Displacement in the xy -plane.

(b) Displacement in the xz -plane.



(c) Displacement in the yz -plane

Figure 6.3: The $l = 2c$ quadrupole mode. Displacement in three planes through a prolate spheroid for the lowest frequency. $d_z = 2$ m, $d_x = 1.5$ m and $d_y = 1.5$ m.

An analytical solution has also been found for this shape (see [13]). It is argued that the condition to get a physically valid solution in the origin can be abandoned. In chapter 3 we have seen that this condition implied that we had to drop the part $\cos(hr)/r$ from the solution (see the remark below formula (3.23)). Because of this extra part Neumann functions (spherical Bessel functions of the second kind) appear in the solutions now. A traction free boundary condition must be imposed on the inner surface as well. Hence expression (3.31) should not only equal zero for $r = a$ but also for $r = b$.

In tables 6.3 and 6.4 the calculated frequencies are compared with the analytical ones. In the first table the quadrupole modes with the lowest frequency are considered for several values of the length of the inner radius. The small values of b are listed because we deal with a hole of similar radius in the detector. The use of the large values is a validation of the numerical approximation method. In the second table values for some other modes are displayed for a fixed b .

d_z (m)	l	$N = 6$	$N = 7$	$N = 8$	$N = 9$
1.00	0	805.111	805.094	805.094	805.094
	1c 1s	804.503	804.461	804.461	804.461
	2c 2s	674.685	674.681	674.681	674.681
1.51	0	651.654	651.649	651.649	651.649
	1c 1s	652.155	652.150	652.150	652.150
	2c 2s	653.627	653.622	653.622	653.622
5.00	0	254.074	254.074	254.074	254.074
	1c 1s	234.923	234.700	234.700	234.700
	2c 2s	593.426	590.836	590.836	590.836
10.0	0	129.572	129.572	129.572	129.572
	1c 1s	74.469	74.438	74.438	74.438
	2c 2s	591.915	585.120	585.120	582.209
15.0	0	86.689	86.689	86.689	86.526
	1c 1s	35.260	35.251	35.251	35.251
	2c 2s	592.836	586.036	586.036	582.378

Table 6.2: The frequencies of the quadrupole modes in Hz when N is increased for a spheroid for a few values of d_z .

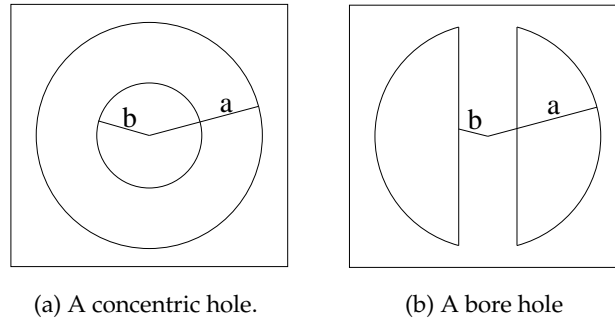


Figure 6.4: Two spheres with different kind of holes. The inner radius is denoted by b and the outer radius by a .

Since the spherical symmetry is conserved, the modes remain degenerate. We can see from table 6.3 that the numerical approximation method gets less accurate if we increase the inner radius. For a small b (0.1 m or less) the method stays accurate.

An important notion is that a hole of macroscopic size introduces a significant frequency shift. This will be a considerable design issue for the resonant mass transducer system of a future gravitational radiation detection system.

b (m)	analytical solution	$N = 6$	$N = 7$	$N = 8$	$N = 9$	$N = 10$
0.075	653.723	653.898	653.891	653.891	653.890	653.890
0.10	653.227	653.637	653.625	653.625	653.623	653.623
0.15	651.221	652.572	652.533	652.533	652.507	652.507
0.75	480.26	502.172	489.503	489.503	486.725	486.725
1.00	393.28	401.950	398.663	398.663	395.301	395.301

Table 6.3: The frequencies of the spheroidal quadrupole modes in Hz for a sphere with a concentric hole.

n	cl.	analytical solution	$N = 6$	$N = 7$	$N = 8$	$N = 9$	$N = 10$
2	1	617.078	617.078	617.078	617.078	617.078	617.078
1	2	892.462	892.470	892.470	892.466	892.466	892.466
3	1	953.499	954.323	953.500	953.500	953.497	953.497
3	2	975.441	975.541	975.541	975.454	975.454	975.454
4	2	1252.01	1281.98	1252.36	1252.36	1252.01	1252.01
4	1	1256.94	1259.45	1259.45	1256.96	1256.96	1256.94
2	2	1261.88	1270.15	1262.87	1262.87	1262.73	1262.73
0	2	1393.36	1395.23	1395.21	1395.21	1395.20	1395.20
1	1	1422.01	1444.82	1422.53	1422.53	1422.01	1422.01

Table 6.4: The analytical and the calculated frequencies in Hz for a few modes of a sphere with a concentric hole. $b = 0.10$ m. The column "cl." indicates whether a mode falls in the first (toroidal mode) or second class (spheroidal mode).

6.4 A bore hole

In this section the sphere is modified with a bore hole. This configuration is drawn schematically in figure 6.4(b). It approximates the suspension hole in the actual detector. The bore hole can be decomposed into a cylinder and two caps at the ends of it. To calculate the volume integral over the basis functions we have to subtract the contributions of the cylinder and the caps from solution 6.1 for the solid sphere. As an analytical solution for the integral over the cylinder with height $2\sqrt{a^2 - b^2}$ and radius b we have

$$\int_{\tau} x^p y^q z^r d\tau = \frac{4\pi b^{p+q+2} (a^2 - b^2)^{\frac{1}{2}(r+1)} (p-1)!! (q-1)!!}{(r+1)(p+q+2)!!} \quad (6.5)$$

A Monte Carlo integration has been implemented to calculate the contribution of the caps. For this purpose the integral is evaluated at 10^5 randomly chosen points in $\frac{1}{4}$ part of a cap.

The results for various values of the radius of the suspension hole are shown in table 6.5 and figure 6.5 for a bore hole around the z -axis. Analogous to the case of the spheroid the modes which transform into each other with a rotation about the z -axis form doublets. Note that the convergence is slightly worse than the case with the concentric hole in the previous

b (m)	l	$N = 6$	$N = 7$	$N = 8$	$N = 9$	$N = 10$
0.05	0	654.015	654.009	654.009	654.008	654.008
	1c 1s	653.346	653.329	653.329	653.323	653.323
	2c 2s	652.609	652.587	652.587	652.576	652.576
0.075	0	653.919	653.908	653.908	653.902	653.902
	1c 1s	652.407	652.360	652.360	652.326	652.326
	2c 2s	650.738	650.670	650.670	650.615	650.615
0.15	0	653.286	653.233	653.233	653.144	653.144
	1c 1s	647.3	646.673	646.673	646.155	646.155
	2c 2s	640.3	639.456	639.456	638.561	638.561

Table 6.5: The frequencies of the quadrupole modes in Hz when N is increased for a sphere with a bore hole for a few values of b .

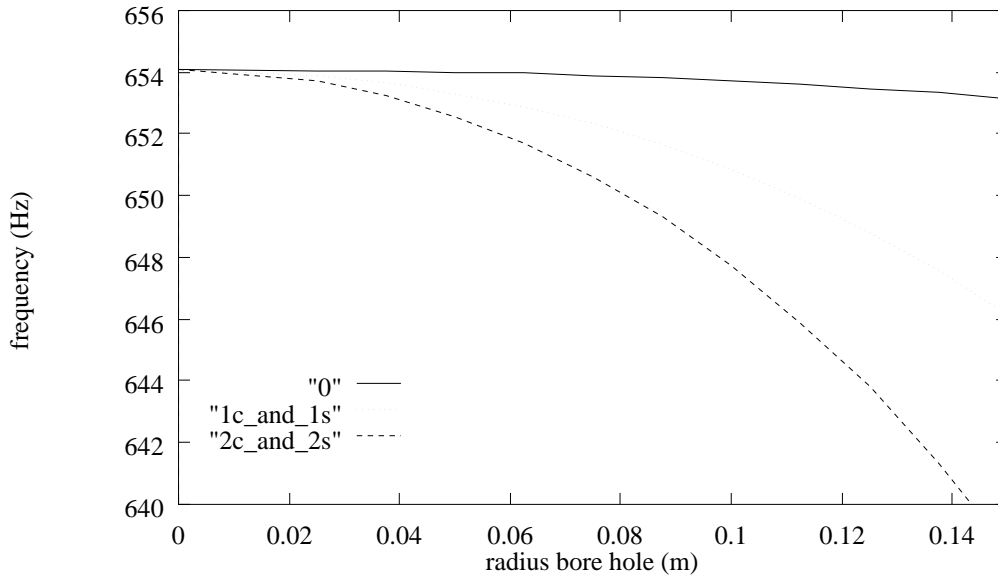


Figure 6.5: The frequencies of the quadrupole modes are shown for a sphere with a suspension hole of radius b . The five modes split into two doublets and a singlet.

section. This can be explained by the fact that we use spherically symmetric trial functions, while our object now possesses cylindrical symmetry. Moreover, sharp edges occur at the boundaries of the hole. Our smooth functions don't fit nicely onto these edges.

We see with this configuration again that the asymmetry fixes the orientation of the eigenmodes. When we make the suspension hole in the direction of another coordinate axis, the eigenmodes rotate accordingly. The unique axis of the prolate-oblate $l = 0$ mode always lines up with the bore hole.

Vector plots are not shown here because they are nearly identical to those for the solid sphere.

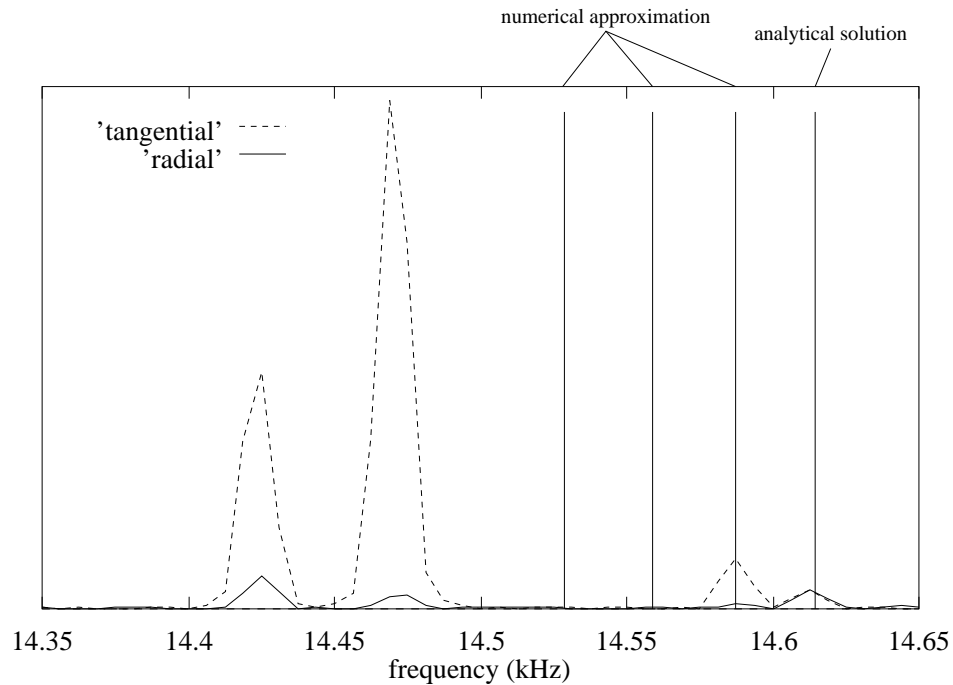


Figure 6.6: The response of the test sphere to a tangential and a radial impulse. The amplitudes of the sphere are compared with the values of the frequencies of the five quadrupole modes obtained with our numerical approximation procedure. The analytical frequency solution for a solid sphere is also indicated. Four peaks are distinguishable for the radial and tangential measurements. The right most one is noise due to the detection system. The other three should match with the three lines from the numerical approximation procedure. The frequency shift for the measurements is much larger than for the calculations.

6.5 Comparison with experimental data

We have the opportunity to compare our calculations with actual measurements. Experiments are performed with a small test sphere. It has a diameter of 15 cm and consists of an alloy of 90% copper and 10% aluminum. The suspension hole has a diameter of 5 mm in the upper half of the sphere and 8 mm in the lower half. The mass is given as 13.1 kg/m^3 . The computer program is modified to deal with a bore hole of two radii. The results are shown in figure 6.6 for the lowest frequency spheroidal quadrupole modes and in figure 6.7 for a larger range of frequencies.

The Lamé parameters of the test sphere were determined to be $\sigma = 0.327$ and $E = 135 \text{ GPa}$ by least square matching of the different columns in figure 6.7.

Some lines do not show up in the case of the measurements in figure 6.7. This is just because not all modes are excited with equal amplitude by applying an impulse on the sphere. Note that the frequency shift is larger in the case of the measurements. This may have several causes. Maybe our approximation for a sphere with a bore hole is not as good as it is for the other shapes treated. It may also be caused by experimental error. For example it may be due to the detection system on the sphere or to inhomogeneities in the test sphere.

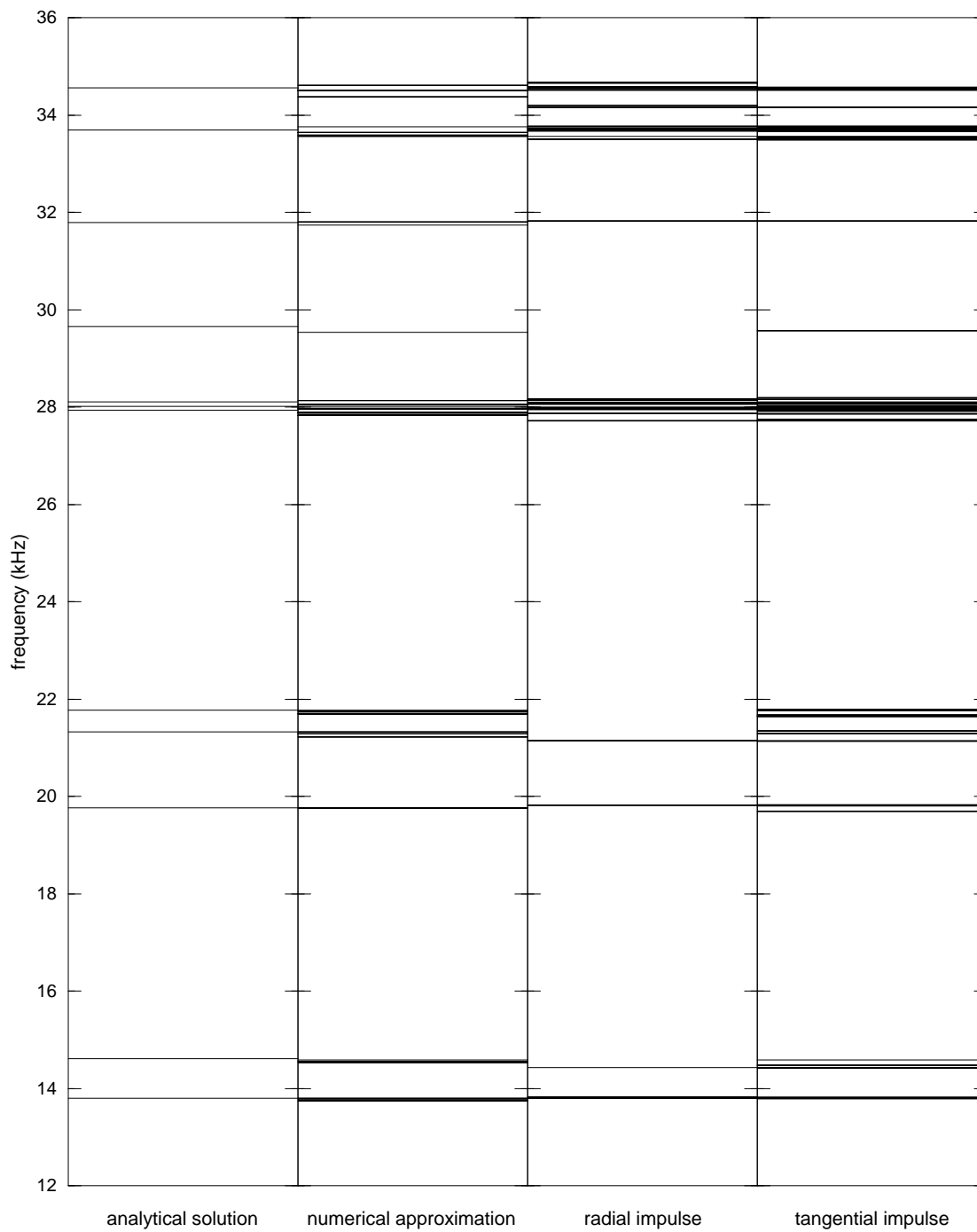


Figure 6.7: A comparison between the analytical solution, the numerical approximation and measurements for the lowest frequencies of a small test sphere. On the left side the analytical frequency solutions for a solid sphere are shown. The next column shows the values obtained with the numerical approximation method. In the other two columns the results of measurements with a test sphere are shown. In one case the sphere is excited by a radial impulse, in the other a tangential impulse is imposed.

Part IV

Conclusions

Concluding remarks and summary

In this thesis we have studied the normal modes of spheres and sphere-like objects. Our main attention was paid to the spheroidal quadrupole modes because these modes are expected to interact with the gravitational radiation field. The vibrations are ruled by the theory of elasticity. This theory with the resulting differential equations was described first. The eigenmodes of homogeneous isotropic freely vibrating spheres could be found by solving these equations analytically. We saw that five degenerate quadrupole modes exist for a solid sphere. For a sphere with the dimensions of the intended GRAIL antenna (i.e. a sphere made of copper with a diameter of 1.5 m) these modes were found to vibrate with a frequency of 654 Hz.

The analytical solutions to the differential equations from elasticity theory were found to be quite complex. It is impossible to solve them in general. Our goal was to study the normal modes of objects with deviations from a spherical shape. Because of the restricted applicability of the analytical solutions we have used a numerical approximation method [15] to calculate the eigenmodes of sphere-like objects. With this method we were able to draw some conclusions about the quadrupole modes for a perturbed sphere:

- When we deform the sphere in an asymmetric way, the degeneracy is partially removed. For example with a bore hole the quintuplet is split into two degenerate doublets and a singlet.
- An asymmetric deviation from the spherical shape fixes the spatial orientation of the quadrupole eigenmodes.
- We expect the frequency shift in the actual detector due to the bore hole to be much larger than the shift arising from other perturbations of the spherical shape. With a bore hole of radius 7.5 cm the frequency changes $\sim 0.5\%$. To reach the same order of magnitude with a deformation into a prolate or oblate spheroid, we have to vary the semi-axes with 1 cm. This is much larger than the expected error arising from casting or deformation by weight.
- Concerning the actual measurements with the GRAIL detector we can state that the frequency shift due to the bore hole is quite large. A rapid loss of phase information because of the frequency splitting of the quadrupole modes must be taken into account. The frequency shift is also a design issue for the bandwidth of the transducer

system. The change of the frequency was found to be even larger in actual measurements.

A few reservations must be made with these conclusions. A number of factors from section 1.2 have not been taken into account. We still don't know the influences of the suspension, the transducers and the strain in the sphere caused by the gravity of the earth.

Moreover, we were not able to make good estimations for the error bounds of the numerical approximation method. We can state that the frequencies of the lowest eigenmodes converge well to a certain value for all the investigated shapes when we took more functions in the expansion. For the solid sphere we saw that the frequencies calculated with the variational method approximated the analytical values well. However, for the shapes for which we lack an analytical solution, we have no guarantee that the calculated value approximates the desired value well.

We would like to have a better understanding of the accuracy of the approximation method for the various perturbations of the spherical shape. Therefore a future research issue could be the investigation of the convergence of the values for the frequencies when the perturbations are made in an arbitrary direction.

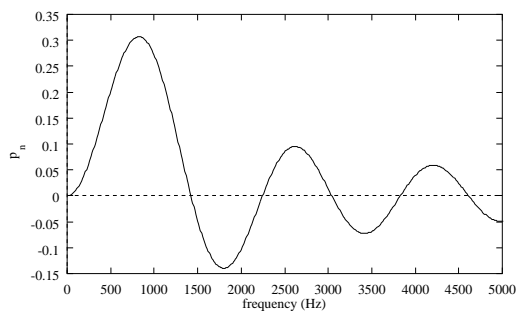
Part V

Appendices

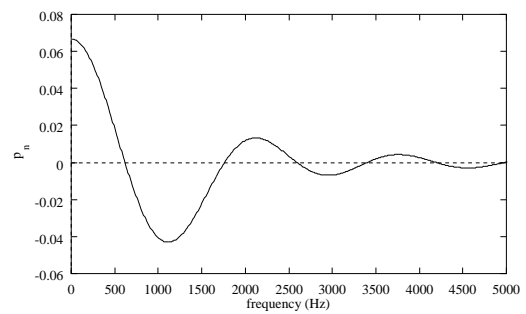
Appendix A

Additional plots

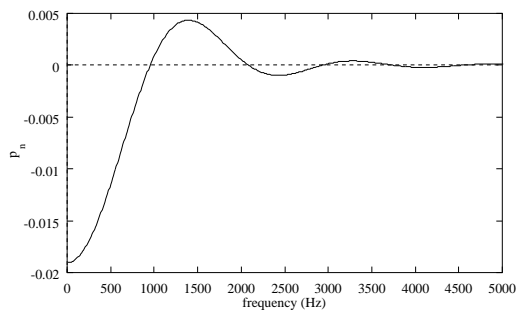
In this appendix plots are shown of the functions p_n and $b_n c_n - a_n d_n$. As is to be seen from equations (3.35) and (3.36) the roots of these functions determine the allowed frequencies of the normal modes of a freely vibrating sphere. The plots are made for a copper sphere with a radius of 1.5 m. The algorithm proposed in [5] has been used for the numerical evaluation of the Bessel functions.



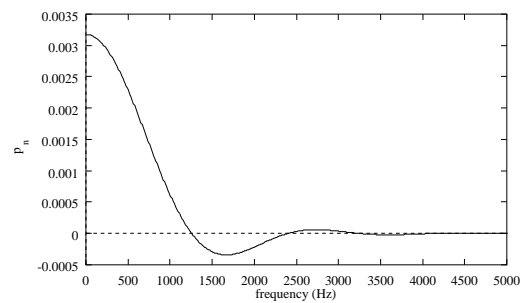
(a) $n = 1$



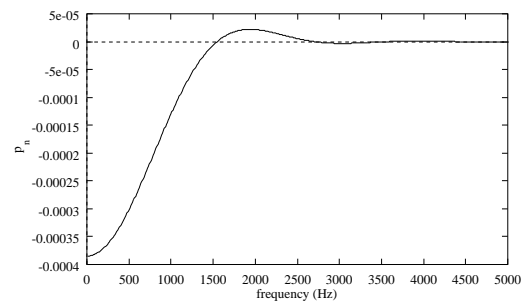
(b) $n = 2$



(c) $n = 3$

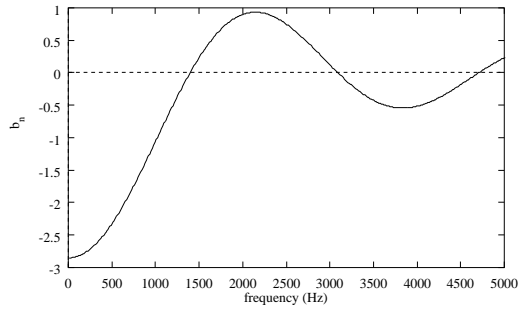


(d) $n = 4$

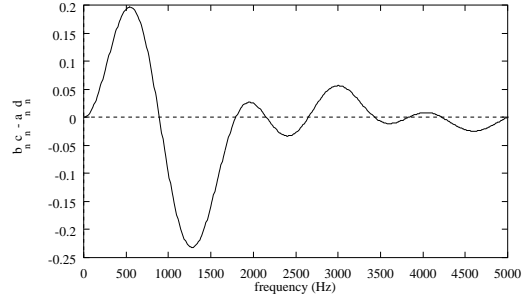


(e) $n = 5$

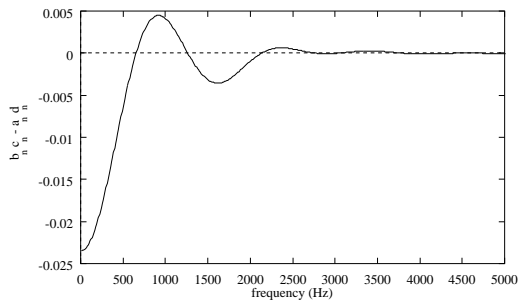
Figure A.1: Vibrations of the first class (toroidal modes). The function p_n whose roots determine the frequencies of the vibrations is plotted for different values of n . See equation (3.33) for an explicit form of p_n .



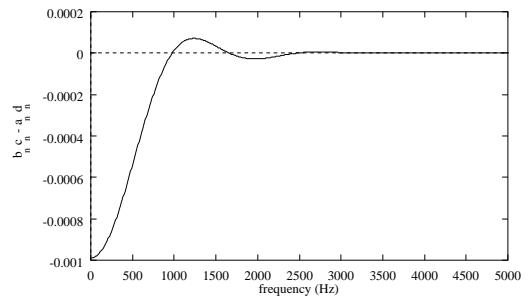
(a) $n = 0$



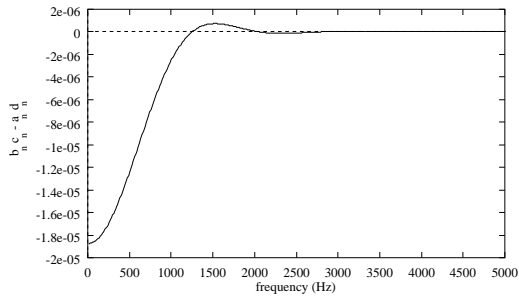
(b) $n = 1$



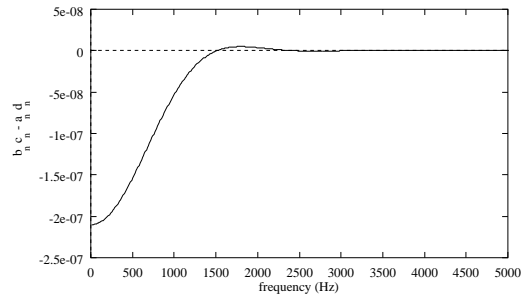
(c) $n = 2$



(d) $n = 3$



(e) $n = 4$



(f) $n = 5$

Figure A.2: Vibrations of the second class (spheroidal modes). The function $b_n c_n - a_n d_n$ whose roots determine the frequencies of the vibrations is plotted for different values of n . See equation (3.33) for explicit expressions for the coefficients.



Appendix B

Documentation for the computer programs

In this appendix the computer programs and tools that were used are described. In the first section we will treat the programs for the numerical approximation procedure. In the second section the implementations of the analytical solutions will be described.

B.1 Numerical approximation

The different FORTRAN programs `Sphere.f`, `Ellipsoid.f`, `SphereConcentricHole.f` and `SphereBoreHole.f` are used to make calculations for the respective objects. They all make use of the same LAPACK [1] routines which in turn make use of BLAS (see [1] and references in there) routines. The files that have to be included for this purpose are called `lapack.f` and `blas.f`. The programs for the numerical approximation can be found in the directory `GRAIL/NumericalApproximation/`

We start to describe how `Sphere.f` works. First the user is asked to enter a value for N . This N occurs in equation (5.9) and defines the truncation of the set of basis functions. If N is chosen to be lower than 5, no useful information will be calculated because not enough basis functions are used. It is also not wise to choose N higher than 8. In this case the double factorial in the denominator of (6.1) will exceed the integer domain*. After a while the program outputs the calculated frequencies to the display and to the file `SphereFrequencies`. Each frequency is assigned a number and an error.

In general two types of errors arise: roundoff error and model error [1]. The first one is due to rounding off results of floating-point operations during the execution of the LAPACK algorithm. Input error is error arising from our own algorithm. Only the roundoff errors are considered here because we don't know how large the error is that arises from the truncation of our set of basis functions.

The user now has the possibility to make one or more files with data which can be used to make plots. A choice between a two dimensional (2D) plot and a three dimensional (3D) plot has to be made first. In the case of a 2D plot the files are suited to make vector plots like

*We could solve this by declaring the function that calculates the double factorial as a double precision type.

figure 4.7. The other case is for drawings like 4.4. The next step is to enter the number of a mode. This number can be looked up in the first column of the file `SphereFrequencies`.

For a 2D plot the file is called `out2D` and is in a Mathematica[†] format. The user must make a choice between one of the three planes that divide the sphere in two equal parts. A package has to be loaded in Mathematica to make a vector plot from the file:

```
<<Graphics`PlotField`
```

Now the command to plot can be given:

```
ListPlotVectorField[<<out2D]
```

Note that the arrows in the figure only give the component of the displacement in that plane.

Three files are made when the 3D option is selected: `total`, `disp` and `place`. A number of points on the surface of the sphere at rest are written to the file `place`. The respective displacements of these points are written to `disp`. The sums of these two values are stored in `total`. To make a plot from the file `total` the following sequence of commands can be given in Mathematica:

```
pts = ReadList["total", Number, RecordLists -> True]
```

```
picture = Table[Map[Point, pts, 1]]
```

```
Show[Graphics3D[ picture]]
```

We have used the other two files to make MPEG movies of the vibrations.

The programs `Ellipsoid.f`, `SphereConcentricHole.f` and `SphereBoreHole.f` work in an analogous way. The differences are as follows. The user is additionally prompted for the length of the three semi-axes in the case of the Ellipsoid. These three axes appear in formula (6.3). The frequencies and errors are written to the file `EllipsoidFrequencies` now. It is not possible to make 3D plots for ellipsoids. For the two programs with a hole in the sphere the user is asked to enter the radius of the hole. The output is respectively written to `SphereConcentricHoleFrequencies` and `SphereBoreHoleFrequencies`.

B.2 Analytical solutions

We have implemented the analytical solutions for the frequencies of the normal modes of a solid sphere in a C program. The file is called `GRAIL/AnalyticalSolutions/CalcEigenFrequencies.c`. The program prints the frequencies of a freely vibrating homo-

[†]Mathematica is a registered trademark of Wolfram Research, Inc. It is a general software system for mathematical and other applications

geneous isotropic sphere. Several options can be given. These options are displayed with the command "CalcEigenFrequencies -h"

Mathematica input files for a sphere with a concentric hole can be found in `GRAIL/Mathematica/`. The files `ConHoleSpher` and `ConHoleTor` can be used for the spheroidal and toroidal modes respectively. `ConHoleSphere` provides us with a function `SpherDet` and `ConHoleTor` provides us with a function `TorDet` when loaded into Mathematica. The roots of these functions determine the frequencies of the normal modes of a freely vibrating sphere with a concentric hole.

Bibliography

- [1] E. Anderson et al. *LAPACK Users' Guide*, second edition, 1994.
- [2] Neil Ashby and Joseph Dreitlin. Gravitational wave reception by a sphere. *Phys. Rev. D*, 12:336–349, 1975.
- [3] Harold H. Demarest Jr. Cube-resonance method to determine the elastic constants of solids. *J. Acoust. Soc. Am.*, 49:768–775, 1971.
- [4] Richard Holland. Resonant properties of piezoelectric ceramic rectangular parallelepipeds. *J. Acoust. Soc. Am.*, 43:988–997, 1968.
- [5] Aleksander Jablonski. Numerical evaluation of spherical bessel functions of the first kind. *J. Comp. Phys.*, 111:256–259, 1994.
- [6] Kaye and Laby. *Tables of Physical and Chemical Constants*. Longman Group Limited, 1986.
- [7] Dr. Günther Landgraf. *Räumliche Probleme der Elastizitätstheorie*. Akademie Verlag Berlin, 1963. Originally by A.I. Lurje. Translated and extended by Dr. Günther Landgraf.
- [8] J. Alberto Lobo. What can we learn about gravitational wave physics with an elastic spherical antenna? *Phys. Rev. D*, 52:591–604, 1995.
- [9] A.E.H. Love. *A Treatise on the Mathematical Theory of Elasticity*. Dover Publications, 1944.
- [10] Stephen M. Merkowitz and Warren W. Johnson. Spherical gravitational wave antennas and the truncated icosahedral arrangement. *Phys. Rev. D*, 51:2546–2558, 1995.
- [11] Stephen M. Merkowitz and Warren W. Johnson. First tests of a truncated icosahedral gravitational wave antenna. *Phys. Rev. Lett.*, (Submitted).
- [12] Eugene Merzbacher. *Quantum Mechanics*. John Wiley and Sons, second edition, 1970.
- [13] NIKHEF, 1996. Internal TR.
- [14] I.S. Sokolnikoff. *Mathematical Theory of Elasticity*. McGraw-Hill book company, second edition, 1956.

-
- [15] William M. Visscher, Albert Migliori, Thomas M. Bell, and Robert A. Reinert. On the normal modes of free vibration of inhomogeneous and anisotropic elastic objects. *J. Acoust. Soc. Am.*, 90:2154–2162, 1991.
- [16] Carl Z. Zhou and Peter F. Michelson. *Spherical Resonant-Mass Gravitational Wave Detectors*. PhD thesis, Physics Department, Stanford University, 1994.